

University of Groningen

## Probes for Non-invasive Matrix Metalloproteinase-targeted Imaging with PET and SPECT

Matusiak, Nathalie; van Waarde, Aren; Bischoff, Rainer; Oltenfreiter, Ruth; van de Wiele, Christophe; Dierckx, Rudi A. J. O.; Elsinga, Philip H.

*Published in:*  
Current Pharmaceutical Design

**IMPORTANT NOTE: You are advised to consult the publisher's version (publisher's PDF) if you wish to cite from it. Please check the document version below.**

*Document Version*  
Final author's version (accepted by publisher, after peer review)

*Publication date:*  
2013

[Link to publication in University of Groningen/UMCG research database](#)

*Citation for published version (APA):*

Matusiak, N., van Waarde, A., Bischoff, R., Oltenfreiter, R., van de Wiele, C., Dierckx, R. A. J. O., & Elsinga, P. H. (2013). Probes for Non-invasive Matrix Metalloproteinase-targeted Imaging with PET and SPECT. *Current Pharmaceutical Design*, 19(25), 4647-4672.

**Copyright**

Other than for strictly personal use, it is not permitted to download or to forward/distribute the text or part of it without the consent of the author(s) and/or copyright holder(s), unless the work is under an open content license (like Creative Commons).

**Take-down policy**

If you believe that this document breaches copyright please contact us providing details, and we will remove access to the work immediately and investigate your claim.

*Downloaded from the University of Groningen/UMCG research database (Pure): <http://www.rug.nl/research/portal>. For technical reasons the number of authors shown on this cover page is limited to 10 maximum.*

# Probes for Non-invasive Matrix Metalloproteinase-targeted Imaging with PET and SPECT

Nathalie Matusiak<sup>1\*</sup>, Aren van Waarde<sup>1</sup>, Rainer Bischoff<sup>2</sup>, Ruth Oltenfreiter<sup>3</sup>, Christophe van de Wiele<sup>3</sup>, Rudi A.J.O Dierckx<sup>1,3</sup> and Philip H. Elsinga<sup>1,3</sup>

<sup>1</sup>Department of Nuclear Medicine and Molecular Imaging, University Medical Center Groningen, University of Groningen, Groningen, The Netherlands; <sup>2</sup>Analytical Biochemistry, Groningen Research Institute of Pharmacy, University of Groningen, Groningen, The Netherlands; <sup>3</sup>Department of Nuclear Medicine, University Hospital Ghent, University of Ghent, Ghent, Belgium

**Abstract:** Dysregulation of matrix metalloproteinase (MMP) activity can lead to a wide range of disease states such as atherosclerosis, inflammation or cancer. The ability to image MMP activity non-invasively *in vivo*, by radiolabelled synthetic inhibitors, would allow the characterization of atherosclerotic plaques, inflammatory lesions or tumors. Here we present an overview of radiolabelled MMP inhibitors (MMPi) and MMP peptides for positron emission tomography (PET) and single photon emission computed tomography (SPECT) for the detection of proteolytic activity of MMPs. So far, most studies are at a preliminary stage; however, some hydroxamate-based tracers such as the peptidomimetics [<sup>111</sup>In]-DTPA-RP782, [<sup>99m</sup>Tc]-(HYNIC-RP805)(tricine)(TPPTS), or Marimastat-ArB[<sup>18</sup>F]F<sub>3</sub> and the picolyl-benzenesulfonamide [<sup>123</sup>I]I-HO-CGS 27023A identified specifically the enzymatic action of MMPs in animal models of various pathologies. The development of new compounds that may lead to novel tracers (e.g. modification of zinc-binding group, variation of substituents attached to the S1', S2' and S3' pockets of the MMP inhibitors) and the use of antibodies and cell penetrating peptides are also discussed. In general, preclinical studies with atherosclerosis models proved to be more successful than those with oncological models.

**Keywords:** MMP inhibitors, MMP peptides, hydroxamates, molecular imaging, PET, SPECT.

## 1. INTRODUCTION

Zinc proteases [1]; [2]; [3], which are the best characterized zinc enzymes, are implicated in many physiological and pathological processes. These proteases are a multi-domain family which is classified based on the structure of their catalytic sites and includes the metzincins, the inuzincins, the gluzincins, the carboxypeptidases, and DD carboxypeptidases (D-alanyl-D-alanine-cleaving carboxypeptidases). The metzincins are defined by a zinc binding consensus sequence **HExxHxxGxxH** which contains three histidine residues and a strictly conserved methionine containing tight 1,4 beta turn (the Met-turn) forming a hydrophobic cleft for the catalytic zinc ion. They are further subdivided according to the residue following the third histidine zinc ligand and the residues surrounding the methionine in the Met-turn. The metzincins comprise the matrixins, the serralsins, the astacins, and the adamalsins. Finally, the matrixins contain the well-known Matrix MetalloProteinases or MMPs and the adamalsins, the A Disintegrin And Metalloproteinases or ADAMs.

### 1.1. Domains of MMPs and ADAMs

MMPs (Fig. 1); [4] are secreted proteins with four distinct conserved domains: the terminal pro-domain, the catalytic domain (which contains a Zn<sup>2+</sup> ion in its active site), the hinge region and the terminal hemopexin domain. Except for MMP-7, MMP-23 and MMP-26, all MMPs contain a hemopexin carboxy-terminal domain. It functions as a recognition sequence for the substrate and stabilizes the interaction of TIMPs (Tissue Inhibitors of Matrix metalloProteinases) with active MMPs [5].

ADAMs (Fig. 1) are membrane bound metzincins. They have a similar structure as the MMPs. The hemopexin domain is replaced by a cystein-rich domain, an EGF (Epidermal Growth Factor)-like domain and the disintegrin domain. The cystein-rich domain and

the disintegrin domain allow ADAMs to interact with proteins connected to the extracellular matrix (ECM) [6].

Under physiological conditions, three forms of MMPs/ADAMs are found, two inactive and one active. The first is the pro-form in which the pro-domain is still present, the second form is inhibited by TIMPs and the third is the active form lacking the pro-domain and not inhibited by TIMPs [7]. The mechanism of action of catalysis of protein substrates is carried out by activation of a zinc-bound water molecule by the carboxylate group of the conserved glutamate residue in the catalytic pocket followed by attack of water on the polarized carbonyl group in the substrate's scissile bond (Fig. 2). Therefore the Zn<sup>2+</sup> ion acts as a Lewis acid [8]. MMPs and ADAMs are activated under the influence of growth factors, hormones, cytokines and cellular transformation [9].

### 1.2. Classification of MMPs and ADAMs

In humans, MMPs form a group of 23 zinc-dependent enzymes (24 in mice) which are generally classified according to their substrate specificity (Table 1); [10]; [11]; [12]. Approximately two-third of the MMPs are secreted as inactive proforms and activated extracellularly. However MMP-11 and membrane-type MMPs are transmembrane metzincins.

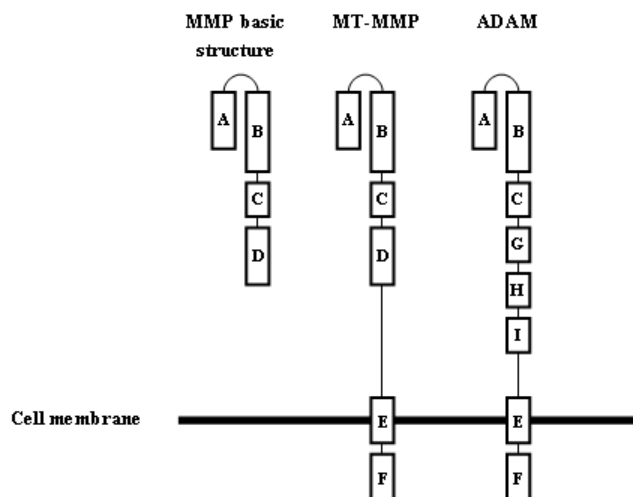
In humans, 22 ADAM proteases have been identified (Table 2); [1]; [6].

### 1.3. Role of the MMP/ADAM family

MMPs and ADAMs are neutral endopeptidases which degrade and remodel structural proteins of the ECM [1]. They are involved in many physiological processes, such as embryo implantation, bone remodelling and organogenesis, and are implicated in the reorganization of tissues during pathological conditions such as inflammation, wound healing and invasion of cancer cells [10].

Upregulation of MMP-2 and MMP-9 is associated with poor prognosis in oncology; therefore, these enzymes are the most widely studied metalloproteinases. MMP-2 degrades type IV collagen and promotes angiogenesis and mitogenesis. The enzyme is overexpressed in many human malignancies and has been associ-

\*Address correspondence to this author at the Nuclear Medicine and Molecular Imaging, University Medical Center Groningen, Hanzeplein 1, 9700 RB Groningen, The Netherlands; Tel: +31 50 3611034; Fax: +31 50 3611687; E-mail: [n.matusiak@umcg.nl](mailto:n.matusiak@umcg.nl)



A: pro-domain, B: catalytic domain, C: hinge region, D: hemopexin domain, E: transmembrane domain, F: cytoplasmic tail, G: disintegrin domain; H: cysteine-rich domain; I: EGF (Epidermal Growth Factor)-like domain.

**Fig. (1).** Schematic representation of the domain structure of MMPs, MT-MMPs and ADAMs

**Table 1.** Classification of the 23 Identified Human MMPs

MMP No.	Enzyme Nomenclature	Principal Substrate(s) <sup>a</sup>	Secreted or Transmembrane Metzincins
MMP-1	Collagenase-1 - Interstitial collagenase	Collagen types I, II, III, VII, and X	Secreted
MMP-8	Collagenase-2 - Neutrophil collagenase	Collagen types I, II, III, VII, and X	Secreted
MMP-13	Collagenase-3	Collagen types I, II, III, VII, and X	Secreted
MMP-2	Gelatinase A - 72 kDa type IV collagenase	Gelatin types I, IV, V, and X; laminin V	Secreted
MMP-9	Gelatinase B - 92 kDa type IV collagenase	Gelatin types I, IV, V, and X; laminin V	Secreted
MMP-3	Stromelysin-1 - Transin-1	Collagen types III, IV, IX, and X; gelatine; pro-MMP-1; laminin; and proteoglycan	Secreted
MMP-10	Stromelysin-2	Collagen types III, IV, IX, and X; gelatin, pro-MMP-1; laminin; and proteoglycan	Secreted
MMP-11	Stromelysin-3	A-1-antiprotease	Transmembrane
MMP-12	Metalloelastase - Macrophage metalloelastase	Elastin	Secreted
MMP-7	Matrilysin-1 - Pump-1	Gelatin, fibronectin and pro-MMP-1	Secreted
MMP-26	Matrilysin-2 - Endometase	To be determined	Secreted
MMP-14	Membrane type-1 MMP - MT1 MMP	Pro-MMP-2, gelatin, and collagens	Transmembrane
MMP-15	Membrane type-2 MMP - MT2 MMP	Pro-MMP-2	Transmembrane
MMP-16	Membrane type-3 MMP - MT3 MMP	Pro-MMP-2	Transmembrane

(Table 1) Contd....

MMP No.	Enzyme Nomenclature	Principal Substrate(s) <sup>a</sup>	Secreted or Transmembrane Metzincins
MMP-17	Membrane type-4 MMP - MT4 MMP	To be determined	Transmembrane
MMP-24	Membrane type-5 MMP - MT5 MMP	To be determined	Transmembrane
MMP-25	Membrane type-6 MMP - MT6 MMP	To be determined	Transmembrane
MMP-19	Human orthologue of <i>Xenopus</i>	Gelatin	Secreted
MMP-20	Enamelysin	Amelogenin (dentine), gelatin	Secreted
MMP-21	Human orthologue of <i>Xenopus</i>	To be determined	Secreted
MMP-23	Cysteine array MMP - Femalysin	To be determined	Secreted
MMP-27	None	To be determined	Secreted
MMP-28	Epilysin	To be determined	Secreted

Table 2. Overview of the 22 Identified Human ADAM Proteases

ADAM	Alternative Names	ADAM	Alternative Names
1	Fertilin $\alpha$ , PH-30 $\alpha$	17	TACE, CD156b Snake venom-like protease
2	Fertilin $\beta$ , PH-30 $\beta$ Cancer/testis antigen 15	18	tMDC III, ADAM-27
3	Cyritestin, tMDC I	19	Meltrin $\beta$ , MADDAM
6	tMDC IV	20	None
7	EAP-1, Sperm maturation-related glycoprotein GP-83	21	ADAM-31
8	Cell surface antigen MS2, CD156a	22	MDC 2
9	MDC9, Meltrin $\gamma$ Myeloma cell metalloproteinase	28	MDC-L, ADAM-23
10	Kuzbanian protein homolog, CD16c	29	Cancer/testis antigen 73
11	MDC	30	None
12	Meltrin $\alpha$	32	None
15	Metargidin, MDC-15	33	None

ated with breast cancers that are metastasizing to the lung. In gelatinase A-deficient mice, tumor-induced angiogenesis was suppressed, melanoma and lung cancer growth were inhibited and the number of lung metastases was reduced significantly [13].

MMP-9 exhibits both anti-cancer and tumor-promoting effects. In animal experiments, disturbance of MMP-9 function decreases tumor development whereas overexpression of MMP-9 induces angiogenesis and increases malignant transformation. Although knock-down of MMP-9 decreased the occurrence of carcinogenesis in certain mouse models, the tumors that were formed in MMP-9 deficient mice were significantly more aggressive and had more undifferentiated phenotypes. This result suggests that MMP-9 may

exert tumor-promoting effects early in the process of carcinogenesis and anti-cancer effects at later stages of the disease [13].

#### 1.4. Inhibition of MMPs/ADAMs

Dysregulation of MMP/ADAM activity is an important aspect of the pathophysiology of several diseases, including atherosclerosis, inflammation and cancer. In addition, MMPs and ADAMs are upregulated in a variety of other diseases such as dermatologic, ophthalmic (macular degeneration), infectious, immunologic, cardiovascular, and neurodegenerative conditions. The control of MMP/ADAM activity by inhibitors has therefore gained considerable interest as a possible therapeutic target [14].

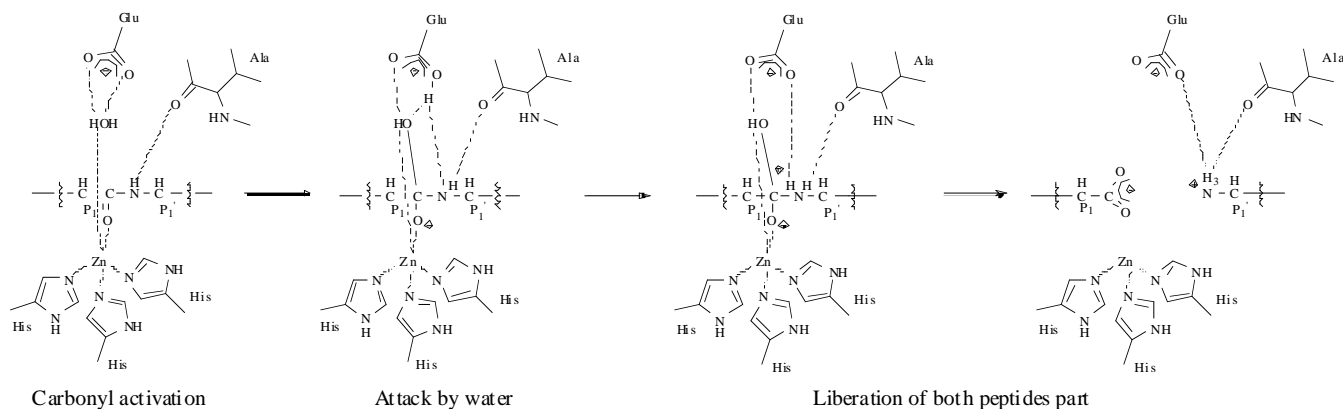


Fig. (2). Mechanism of action of catalysis of protein substrates by MMPs.

MMPs and ADAMs are inhibited by nonspecific protease inhibitors such as  $\alpha_2$ -macroglobulin and  $\alpha_1$ -antitrypsin, and by a small family of specific natural inhibitors towards metalloprotease activity: TIMPs. These physiological inhibitors, which form a group of 4 glycoproteins (TIMP 1-4) (21-30 kDa in size), have affinities for MMPs in the  $10^{-10}$  to  $10^{-16}$  M range and seem ideal candidates for labelling and therapy but they lack selectivity and possess other biological functions [10]; [15]; [16]. For instance, they stimulate growth of several cell types, induce changes in cell morphology and inhibit angiogenesis [12]. As a result, synthetic and more specific MMP inhibitors (MMPIs) were developed. The following structural features are required to design an MMPI:

- at least one functional group that provides a hydrogen bond interaction with the enzyme backbone,
- one or more side chains, capable of van der Waals interactions with the enzyme subsites and
- a functional group (e.g., hydroxamate, phosphonate, carboxylate, thiol, barbiturate, etc.) capable of chelating the active-site zinc(II) ion (referred to as zinc binding group or ZBG) (Fig. 3); [11]; [17]; [18].

By structure-activity relationship (SAR) studies and combinatorial chemistry, a schematic representation of the binding mode of a peptidomimetic MMP/ADAM inhibitor (Fig. 4) was proposed. Three different binding pockets were defined. First of all, the S1' pocket, commonly called the "selectivity pocket", is a relatively deep pocket for the majority of the enzymes except for MMP-1, -7 and -11. A "more" selective inhibitor is obtained when a large substituent (mainly hydrophobic) is attached to it while smaller P1' substituents (generally aliphatic) resulted in a broad-spectrum inhibitor. The S2' pocket is a solvent-exposed pocket which has more affinity for hydrophobic P2' residues. Then, the S3' pocket is an ill-defined solvent-exposed region. Finally, activity of some MMP members can be increased by incorporating a substituent in the alpha position of the zinc-binding group of a MMPI [11]; [19].

### 1.5. Quantification of MMPs

Up to now, most research linking MMPs to diseases has been restricted to *ex vivo* assays on excised tissues or fluid samples using fluorescence detection kits, immunohistochemistry, ELISA, zymography, or Western blotting, addressing the correlation between protein quantity (immunological assays) or expression levels (mRNA analysis) and disease activity or state. As proteolytic activity is highly regulated and used as a marker for certain cancer types or inflammation, molecular imaging of locally up-regulated and activated matrix metalloproteinases *in vivo* could be used to improve the early detection of diseases, to image the efficacy of prote-

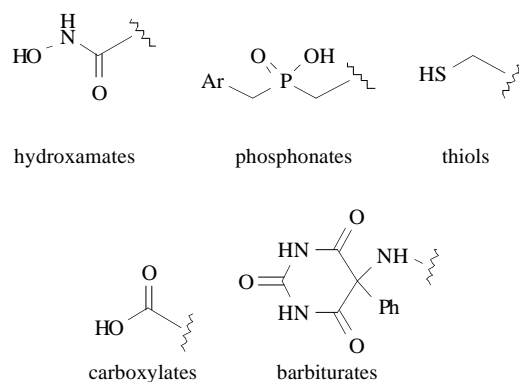


Fig. (3). Structure of ZBGs in MMP/ADAM inhibitors.

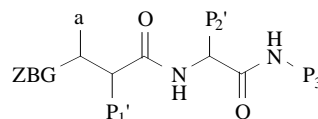


Fig. (4). Schematic representation of a peptidomimetic MMP/ADAM inhibitor.

ase inhibitors, to serve as an *in vivo* screening tool for drug development, to image transgene expression, or to understand how protease activities are regulated [20].

Here we review MMP inhibitors, MMP peptides, antibodies, as well as cell-penetrating peptides for the detection of proteolytic activity of MMPs and ADAMs, using single photon emission computed tomography (SPECT), and positron emission tomography (PET).

## 2. PROBES FOR IMAGING MMPs

### 2.1. MMP Inhibitors for PET/SPECT

#### 2.1.1. Natural MMP Inhibitors

Logically, radiolabelled endogenous TIMPs were chosen as a target for the diagnosis of pathologies associated with upregulated MMP levels. TIMPs bind noncovalently to MMPs with binding at very high  $K_d$  values [7]. Each TIMP is composed of two domains, the N- and C-terminal, which are both characterized by three disulfide bonds [21]. Among the TIMP family, TIMP-2 has generated the most interest because the N-terminal domain of TIMP-2 (N-TIMP-2) folds in the absence of the C-terminal domain and main-

tains inhibitory activity [22]. Moreover, N-TIMP-2 has affinities for MMPs in the  $10^{-12}$  to  $10^{-9}$  M range which is much higher than synthetic MMP inhibitors (usually  $10^{-9}$  M). TIMP-2 demonstrated positive effects in a variety of animal models of disease such as ovarian cancer [23].

### [<sup>111</sup>In]-DTPA-N-TIMP-2, 1

Giersing *et al.* [24] conjugated the N-terminal domain of recombinant human TIMP-2 (127 amino acids) with the bifunctional chelator diethylenetriamine pentaacetic acid (DTPA) followed by radiolabelling to obtain [<sup>111</sup>In]-DTPA-N-TIMP-2 **1**. Fluorogenic inhibition assay with the catalytic domain of MMP-3 (cMMP-3) was performed with N-TIMP-2 and **1**. N-TIMP-2 and **1** inhibited cMMP-3 identically, which suggested no effect from the radiolabelling.

As dysregulation of MMP expression was correlated with Kaposi sarcoma (KS) development and no tracer so far was able to detect specifically this pathology, Kulasegaram *et al.* [25] performed a pilot study with **1** in five patients with HIV infection and KS. Patients did not exhibit significant retention of **1** in the established KS lesions.

### [<sup>123</sup>I]-rhTIMP-2, 2

As radiolabelling of rhTIMP-2 with [<sup>111</sup>In]-DTPA could lead to a random DTPA-conjugate, Oltenfreiter *et al.* [26] performed iodination of rhTIMP-2 with Na<sup>123</sup>I in order to obtain [<sup>123</sup>I]-rhTIMP-2 **2**. Biodistribution in NMRI mice after administration of [<sup>123</sup>I]-rhTIMP-2 was performed. **2** exhibited no long-term accumulation in heart, lungs, liver and heart. A rapid clearance by the kidneys was obtained due to the low molecular weight of rhTIMP-2 (21 kDa). The stomach showed a retention of 24.5% ID/g 1 hr p.i. suggesting dehalogenation of **2**.

Since N-TIMP-2 was shown to bind specifically MT1-MMP, van Steenkiste *et al.* [27] evaluated **2** on MT1-MMP-overexpressing (S.1.5) and control (C.IV.3) tumor-inoculated mice. TIMP-1 exhibits similar binding as TIMP-2 towards soluble MMPs. However TIMP-1 was unable to bind MT1-MMP and was used as negative control. Preliminary studies with tumor-free nu/nu mice indicated a comparable clearance rate for **2** and [<sup>123</sup>I]-rhTIMP-1. Planar imaging allowed visualizing **2** in S.1.5 tumor in contrast to contralateral background areas. Each time point demonstrated significant differences between **2** and [<sup>123</sup>I]-rhTIMP-1 in S.1.5 tumor and **2** in S.1.5 and C.IV.3 tumors. Although evaluation to demonstrate the specificity of [<sup>123</sup>I]-rhTIMP-2 is necessary, **2** may be a potential tracer to visualize tumor associated with MT1-MMP overexpression.

Even though [<sup>111</sup>In]-DTPA-N-TIMP-2 and [<sup>123</sup>I]-rhTIMP-2 represent attractive tracers for imaging of MMP activity, no further evaluation was performed. Partially due to the difficult purification of N-TIMP-2, synthetic MMP inhibitors attracted much more interest.

## 2.2. Synthetic MMP Inhibitors with a ZBG

The synthetic MMPs are classified on the basis of the group that binds to the zinc atom: hydroxamate, carboxylate or barbiturate.

### 2.2.1. Hydroxamate-based MMP Inhibitors

Most of the MMP/ADAM inhibitors belong to the hydroxamate category. Hydroxamic acid is a functional group which corresponds to a hydroxylamine inserted into a carboxylic acid. The hydroxamate is the most potent ZBG, the strength of the binding results from a five membered ring in which both oxygens are bound to the metal center [28] (Fig. 5). It acts as a bidentate ligand with the active-site zinc ion. We subdivided these MMPIs into two categories peptidomimetic hydroxamates and nonpeptidomimetic sulfonamide hydroxamates.

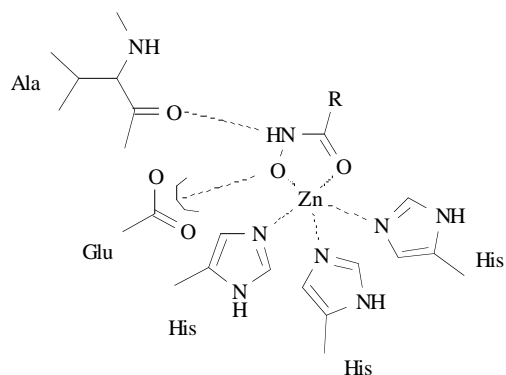


Fig. (5). Binding pose of the hydroxamate ZBG into the active site of MMPs.

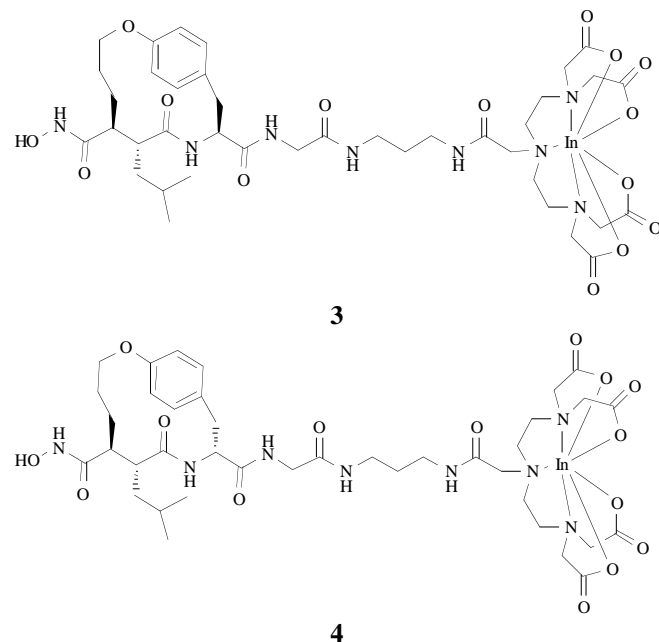
### Peptidomimetic Hydroxamate Inhibitors

Peptidomimetics mimic the structure of collagen (a substrate of MMP) at the MMP cleavage site. These compounds function as competitive inhibitors and chelate the zinc atom of the MMP enzyme activation site [13].

### [<sup>111</sup>In]-DTPA-RP782, 3; [<sup>111</sup>In]-DTPA-RP788, 4; and [<sup>99m</sup>Tc]-HYNIC-RP805(tricine)(TPPTS), 5

Su *et al.* [29] performed preliminary nonimaging studies with [<sup>111</sup>In]-DTPA-RP782 **3** and the negative control [<sup>111</sup>In]-DTPA-RP788 **4** (Fig. 6), RP788 being the biologically inactive isomer of RP782. Both SPECT-tracers were tested in control mice and in mice one week after myocardial infarction (MI) surgery. Microautoradiography allowed the detection of [<sup>111</sup>In]-DTPA-RP782 in the MI, in contrast to [<sup>111</sup>In]-DTPA-RP788 (Fig. 7). **3** and **4** showed similar myocardial uptake in control mice.

A technetium tracer based on an analog inhibitor of **3** was synthesized: [<sup>99m</sup>Tc]-HYNIC-RP805(tricine)(TPPTS) **5** (Fig. 6). MMP fluorogenic assays were performed on the macrocyclic inhibitor RP805. RP805 showed nanomolar affinities *in vitro* against MMP-2, MMP-3, MMP-7, MMP-9, MMP-12, MMP-13, ADAM-10 and ADAM-17 (Table 3). Compound **3** and **5** were evaluated in various settings.



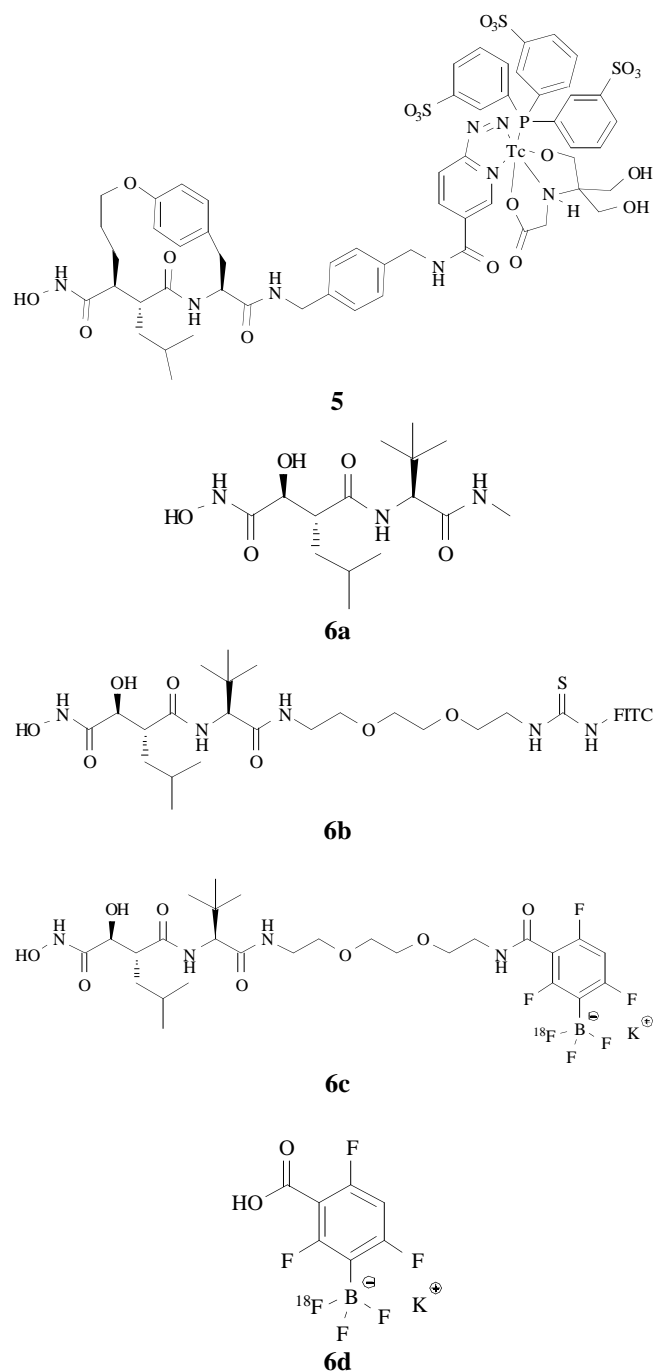


**Fig. (6).** Structure of peptidomimetic hydroxamate-based MMP inhibitors for PET/SPECT.

### Vascular Remodeling Imaging

Su *et al.* [29] evaluated **5** in mice one, two and three weeks after MI surgery and in control mice with microSPECT/CT. About 5-fold increase of **5** uptake in the infarct region was obtained in mice having undergone MI surgery (after 1, 2 and 3 weeks) in contrast to control mice. Myocardial [<sup>99m</sup>Tc]-(HYNIC-RP805)(tricine) (TPPTS) activity in the remote noninfarcted area was approximately 2-fold higher than in control mice, this difference being statistically significantly different at two and three weeks. In control mice, immunofluorescent staining was minimal for MMP-2 and absent for MMP-9 whereas for mice after MI, strong staining was

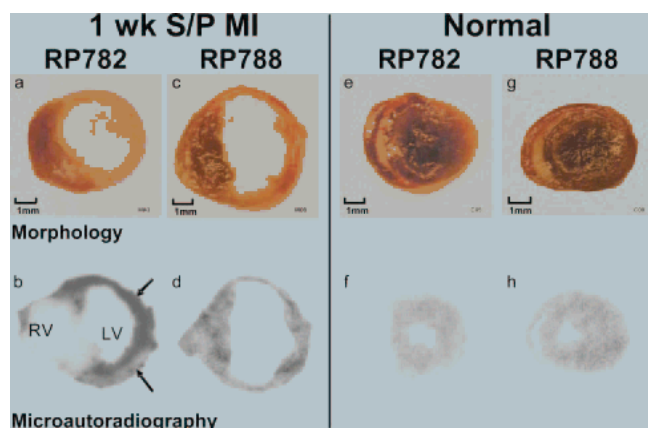


**Fig. (7).** Morphology and **3** and **4** microautoradiography of short-axis myocardial sections of mice at one week after MI and control mice.

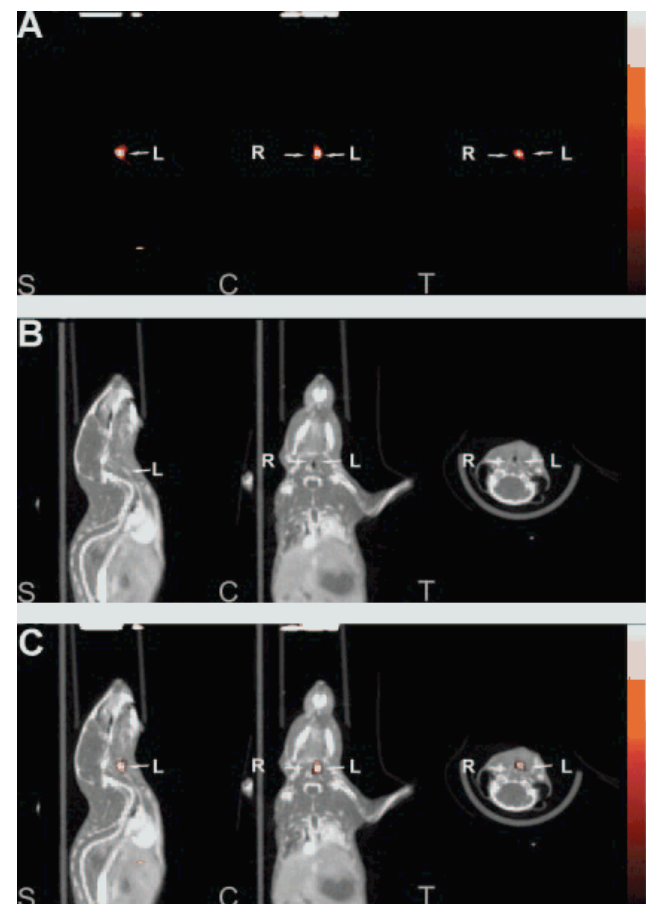


**Fig. (8).** Example of (A) **3** microSPECT, (B) CT angiography, and (C) fused microSPECT/CT *in vivo* imaging at 3 weeks after carotid injury. L: left carotid artery - R: right carotid artery.

obtained for both gelatinases. Moreover, the fluorescence was significantly related to the MI region and was confirmed by zymography.

Zhang *et al.* [30] evaluated **3** in injury-induced vascular remodeling in mice. ApoE<sup>-/-</sup> mice after one week of high-cholesterol (HC) diet underwent left common carotid injury. The right carotid was used as control. Specificity of **3** was tested with a 50-fold excess of unlabelled precursor RP782. Staining of the carotid wire injury resulted in significant hyperplasia and expansive remodeling over a

Table 3. IC<sub>50</sub> Values of Synthetic MMP Inhibitors/MMP Peptides

MMP inhibitors / MMP peptides	IC <sub>50</sub>																	
	MMPs														ADAMs			
	MMP-1	pro-MMP-2	MMP-2	MMP-3	MMP-7	MMP-8	pro-MMP-9	MMP-9	mMMP-9	MMP-12	MMP-13	MMP-14	cMT1	cMT3	ADAM-10	ADAM-17		
RP805 [29]; [31]; [32]; [33]; [34]; [35]; [37]; [38]; [39]			10.5 nM	14 nM	< 6.4 nM				7.4 nM								27 nM	95 nM
6a [40]; [41]			2.02 nM															
6b [40]; [41]			7.70 nM															
6c [40]; [41]			1.59 nM															
Br-7 [42]; [43]		0.5±0.1 nM						4.9±3.1 nM						25.0±6.2nM	7.0±4.6nM			
7 [42]; [43]		0.6±0.05 nM						2.4±1.4 nM						21.7±6.4 nM	7.3±0.6 nM			
8 [44]; [45]		48±2 nM						740±62 nM						2509±342 nM	973±150 nM			
9 [46]	43 nM	11 nM	34 nM			13 nM		27 nM		4.9 nM								
11 [46]	33 nM		20 nM	43 nM				8 nM										
12a [50]; [51]			4±3 nM			2±1 nM		50±27 nM				11±0.3 nM						
15a [54]			320 nM					153 nM										
15d [54]			2.5 nM					4.6 nM										
16 [51]; [56]			3±1 nM			2±1 nM		7±1 nM				0.8±0.03 nM						
17 [50]; [57]			8±1 nM			0.9±0.3 nM		0.5±0.1 nM				0.9±0.2 nM						
18 [58]			0.13±0.07 nM			0.02±0.004 nM		0.03±0.003 nM				0.006±0.003 nM						
19 [47]	1.5 μM		3 nM	8 nM	7.2 μM			2.2 μM				6 nM						
22 [60]			110 nM					200 nM										
Br-23 [42]; [43]		7.3±0.6 nM						239.7±15.7 nM						437.0±22.6 nM	252.3±12.2 nM			
23 [42]; [43]		9.3±1.5 nM						201.0±58.6 nM						859.0±31.1 nM	678.7±45.3 nM			
24 [44]; [45]		23±3 nM						429±36 nM						180±45 nM	232±29 nM			
25a [61]			1.9 μM															
27 [65]			7 nM					2 nM										
28 [66]	> 50 μM		23±9 nM			138±12 nM		7±2 nM				645±17 nM	760 μM					
29 [67]			58±14 nM			58±3 nM		27±6 nM				51±11 nM						



(Table 3) Contd....

MMP inhibitors / MMP peptides	IC50															
	MMPs														ADAMs	
	MMP-1	pro-MMP-2	MMP-2	MMP-3	MMP-7	MMP-8	pro-MMP-9	MMP-9	mMMP-9	MMP-12	MMP-13	MMP-14	cMT1	cMT3	ADAM-10	ADA-M-17
31 [69]; [71]			13.2±1.6 μM			NI		9.6 μM	11.0±2.5 μM		NI	NI				
32 [70]			5 to 10 μM					50 to 100 μM								
33 [71]			8.7 μM					8.6 μM	18.2 μM							
34 [71]			> 1000 μM						20.4 μM							
35 [72]			1026 μM													

NI no inhibition

period of 4 weeks. From one week after surgery, zymography supported that wire injury induced a measurable increase in MMP-2 and MMP-9 activity, which was highest at 3 weeks. Retention of **3** in injured carotid arteries was visualized at 2, 3 and 4 weeks after surgery (Fig. 8). Pre-blocking of binding in mice resulted in a substantial reduction in retention of **3**. Blocking of sections of left-carotid arteries at 3 weeks after surgery with the broad spectrum MMPI 1,10-phenanthroline (10 mmol/L) significantly inhibited binding of **3**. Finally, an excellent correlation was obtained between uptake of **3** and weekly variations in the vessel wall cross-sectional area but not with modifications in the total vessel or luminal areas.

Tavakoli *et al.* [31] evaluated **5** in ApoE<sup>-/-</sup> mice under high fat diet which received left common carotid artery wire injury. Two weeks after surgery, mice fed high cholesterol diet with carotid surgery, showed significantly higher uptake in the left carotid artery, compared to sham-operated mice or right carotid artery of both groups. [<sup>99m</sup>Tc]-[HYNIC-RP805](tricine)(TPPTS) retention was significantly reduced after diet withdrawal (Fig. 9). A longitudinal study showed persistence of the tracer uptake in the left carotid in high fat diet mice after two and four weeks of surgery. Removal of the high fat diet resulted in a significant decrease of retention of **5** in the left carotid. Significant decrease in MMP-2, -3, and -13 expression levels in injured arteries was obtained in mice with high fat diet withdrawal. Only MMP-12 remained significantly elevated in the injured artery in the withdrawal group. Removal of the high fat diet led to a significant decrease in left carotid neointima formation compared to high fat diet mice. Finally, high fat diet animals showed a significant increase in monocyte/macrophage infiltration in contrast to sham-operated mice.

Sahul *et al.* [32] analysed pigs, which underwent MI, with MRI and SPECT/CT imaging with **5**. The left ventricular (LV) end diastolic volumes were significantly higher at each time point compared to control pigs. Pigs at 1, 2 and 4 weeks after surgery showed retention of **5** in the posterolateral wall, with a maximal uptake at 2 weeks post-MI. *Ex vivo* imaging of LV slices substantially correlated with the *in vivo* accumulation of **5** in the region of perfusion defect even if some tracer uptake was also obtained in remote regions 1 and 2 weeks after surgery. An increase in uptake of **5** was obtained in all myocardial regions after 1 and 2 weeks MI surgery, with 4 times higher retention in the infarct region compared to controls. Pigs at 4 weeks post-MI had similar uptake of **5** in the remote area than control pigs but showed higher accumulation in the infarct and border regions compared to controls. Zymography demonstrated the expression of MMP-2, -7, -9 and -14 at each time point

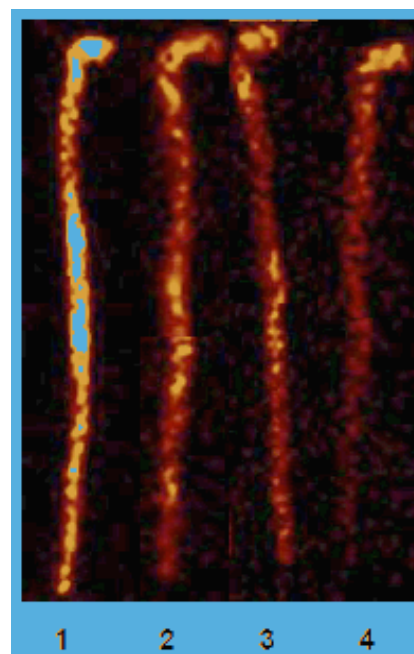


Fig. (9). Fused microSPECT/CT images of mice, administered with **5**, 2 weeks after left common carotid artery wire injury with a high fat diet or diet withdrawal.

and different areas of myocardial segments; in addition an exponential correlation between the post MI-change in LV end diastolic volume and MMP activity was found by using a specific global MMP fluorogenic substrate. *Ex vivo* MMP-2 activity showed the best correlation with regional uptake of **5**.

#### Atherosclerotic Lesions Imaging

Fujimoto *et al.* [33] tested **5** in rabbits with atherosclerotic lesions with SPECT/CT. Control rabbits did not show any accumulation of the tracer. **5** was clearly visualized in atherosclerotic lesions. In blocking experiments, [<sup>99m</sup>Tc]-[HYNIC-RP805](tricine)(TPPTS) uptake in atherosclerotic lesions was reduced in a dose-dependent manner. The tracer uptake was also significantly reduced after diet withdrawal and fluvastatin treatment (cholesterol-lowering drug) (1.0 mg/kg). *Ex vivo* gamma imaging studies of harvested aortas

confirmed the *in vivo* SPECT/CT imaging (Fig. 10). In addition, the retention of **5** was correlated with immunohistochemistry of macrophages, MMP-2 and MMP-9 in atherosclerotic plaques.

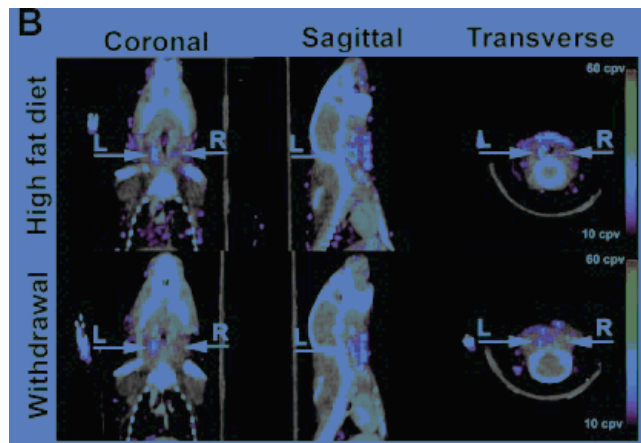


**Fig. (10).** Ex vivo images of explanted aortas of (1) HC diet, (2) fluvastatin treatment, (3) diet withdrawal and (4) control animals administered with **5**.

Ohshima *et al.* [34] investigated **5** in mice deficient in apolipoprotein E (apoE<sup>-/-</sup>), mice deficient in low-density-lipoprotein receptor (LDLR<sup>-/-</sup>) and in control mice. Half of the apoE<sup>-/-</sup> mice and half of the LDLR<sup>-/-</sup> mice received a high-cholesterol diet. **5** showed the highest uptake in atherosclerotic lesions in apoE<sup>-/-</sup> mice with a high-cholesterol diet, followed by LDLR<sup>-/-</sup> mice with high-cholesterol diet, apoE<sup>-/-</sup> mice fed with a normal chow and LDLR<sup>-/-</sup> mice with normal chow. Control mice presented the lowest retention (Fig. 11). Immunohistochemistry with the fluorescent staining of MMP-2, MMP-9 and macrophages correlated significantly with the uptake of **5**.

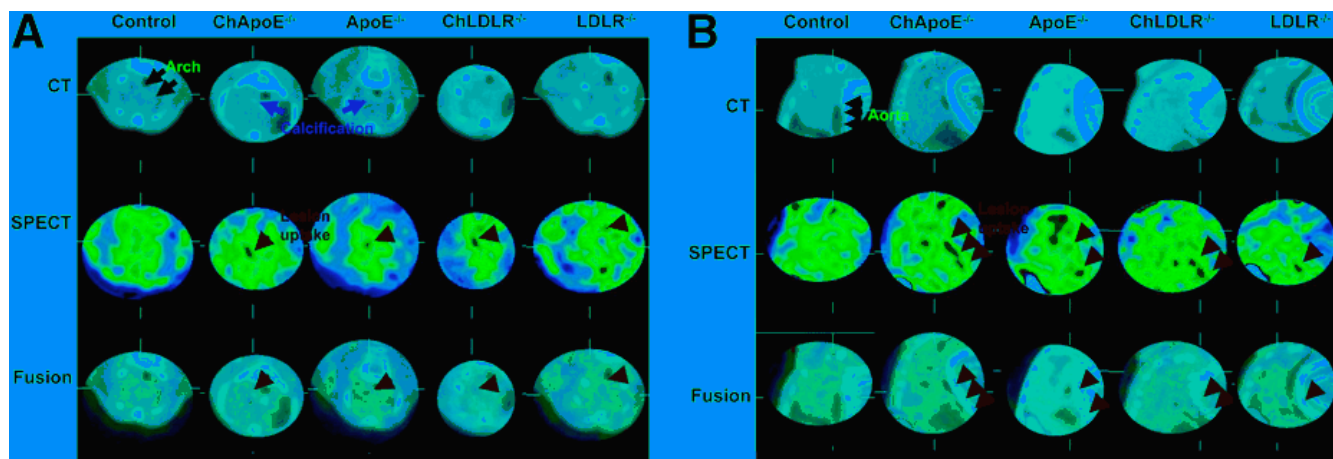
Ohshima *et al.* [35] evaluated the effect of fluvastatin and minocycline (an antimicrobial agent which exhibits significant MMP inhibitory activity) either separately or in combination in rabbits with atherosclerotic lesions injected with **5**. Highest retention of **5** was observed in unmanipulated rabbits. A significant decrease was observed in the fluvastatin (1.0 mg/kg), high dose of minocycline (3.0 mg/kg) and a combination of low-dose minocycline (1.5 mg/kg) and fluvastatin. **5** was not significantly decreased in the low dose minocycline group. No synergistic effect was obtained for the

combination of low-dose minocycline and fluvastatin. The tracer uptake was significantly correlated with MMP-2 and MMP-9 staining.

Razavian *et al.* [36] tested **3** in atherosclerotic mouse aorta after dietary modification. Retention of **3** was significantly higher in the aorta than in the inferior vena cava (IVC) *in vivo*, with the highest accumulation in the proximal aorta. *In vivo* and *ex vivo* quantification of **3** in the aorta resulted in a significant correlation. Oil red O staining of explanted areas showed a satisfactory concordance between atherosclerosis area and retention of **3**; even if zones of divergence were found. Mice from one month to three months high fat diet presented a progressive increase of [<sup>111</sup>In]-DTPA-RP782 uptake along the aorta. Heterogeneity of **3** along the aorta increased over time. Pre-treatment with a 50-fold excess of nonlabeled precursor led to a significant reduction in tracer accumulation in the aorta. Oil red O staining showed that getting back to normal chow after two months of high fat diet resulted in about 30% reduction in the relative plaque area. A substantial and much more pronounced decrease in tracer uptake was obtained in the withdrawal group. A significant correlation was found between expression of MMP-2, -3, -12 and -13 with uptake of **3** *in vivo*. However, MMP-9 did not show any substantial concordance. Dietary modification resulted in a significant decrease in MMP-2, -3, -12 and -13 (not MMP-9) in the proximal aorta. RT-PCR in aortae showed that even if a significant correlation was obtained between CD31 (endothelial cells) or SM  $\alpha$ -actin (vascular smooth muscle cells) expression and uptake of **3**; CD68 and EMR-1 expression (reflecting the presence of macrophages) was substantially correlated with tracer retention. Dietary modification did not affect CD31 and SM  $\alpha$ -actin expression however it significantly decreased aortic CD68 and EMR-1 expression.

Haider *et al.* [37] examined the relation between apoptosis and MMP release in a model of atherosclerosis in rabbits. Dual radionuclide imaging was performed with **5** and [<sup>111</sup>In]-labeled annexin A5 (AA5) (Fig. 12). The retention of **5** and AA5 was substantially higher in rabbits fed a high cholesterol diet than in controls. **5** and AA5 uptake decreased significantly in rabbits after fluvastatin treatment (1.0 mg/kg) and diet withdrawal. MMP-9, macrophages, TUNEL (terminal deoxyribonucleotide transferase-mediated nick-end labeling) staining were significantly correlated with **5** and AA5 uptake. In addition, culture medium apoptotic THP-1 monocytes confirmed MMP-9 release which suggests that apoptosis and MMP are interconnected in atherosclerotic lesions.

As MMP expression and apoptosis are both involved in early and in advanced atherosclerotic plaques, **5** and [<sup>99m</sup>Tc]-(HYNIC-



Ch: high-cholesterol-fed

**Fig. (11).** *In vivo* microSPECT/CT transverse (A) and sagittal (B) images of the five groups of animals

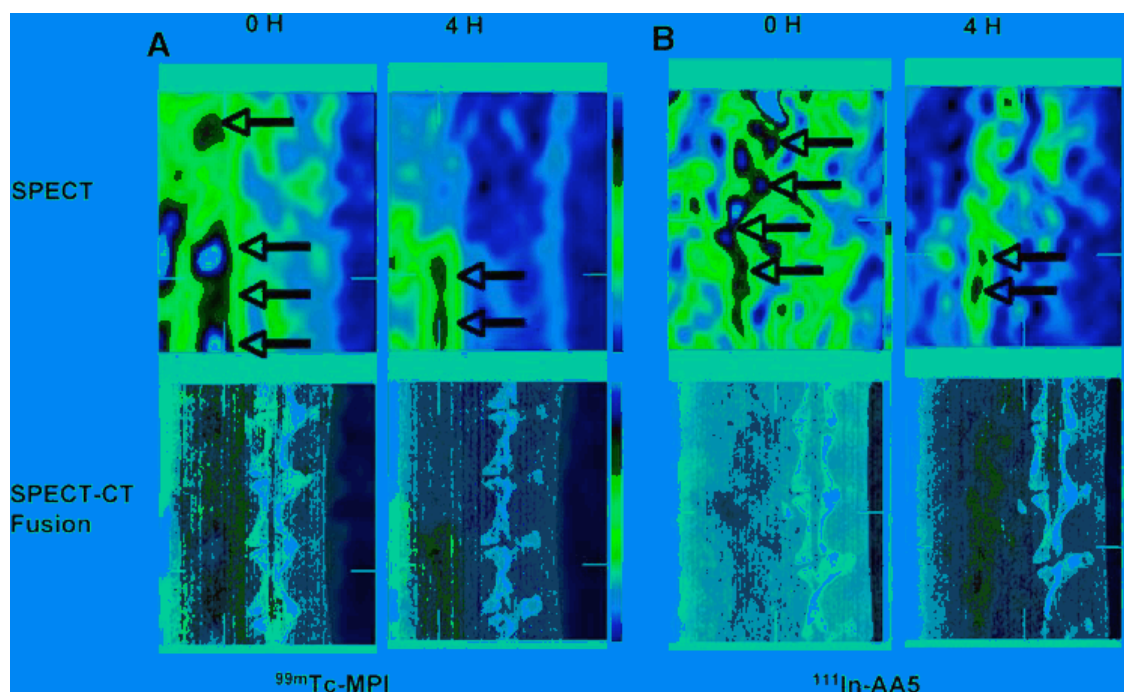


**Fig. (12).** Example of microSPECT and fused microSPECT/CT images of atherosclerotic rabbits under HC diet injected with **5** or AA5.

Annexin V)(tricine)<sub>2</sub> were tested to characterize more advanced atherosclerotic disease in apoE<sup>-/-</sup> mice [38]. In the youngest group of apoE<sup>-/-</sup> mice, neither **5** nor [<sup>99m</sup>Tc]-(HYNIC-Annexin V)(tricine)<sub>2</sub> accumulated in the chest or neck and showed minimal lesion (Fig. 13). In aortic lesions, at 20 weeks, retention of [<sup>99m</sup>Tc]-(HYNIC-Annexin V)(tricine)<sub>2</sub> was slightly higher than **5** and at 40 weeks **5** showed significantly higher uptake than annexin V 20 and 40 week-old mice showed significantly higher uptake of **5** compared to [<sup>99m</sup>Tc]-(HYNIC-Annexin V)(tricine)<sub>2</sub> in carotid. A substantial correlation was found between %ID/g of Annexin V with % macrophages and caspase-3 positive cells. %ID/g of **5** showed also a significant relationship with % macrophages and with MMP-2 and -9 positive cells. No *ex vivo* correlation was possible due to the low number of animals. To conclude: **5** allowed to identify more advanced atherosclerotic lesions than [<sup>99m</sup>Tc]-(HYNIC-Annexin V)(tricine)<sub>2</sub>.

#### Aneurysm Imaging

Razavian *et al.* [39] evaluated **3** and **5** in murine carotid aneurysm. Arterial aneurysm was obtained by exposing the left common carotid artery of apoE<sup>-/-</sup> mice fed HC chow since 1 week to CaCl<sub>2</sub>. The right carotid artery was exposed to saline and was used as a control. Mice were scanned with **3** 2, 4 or 8 weeks after surgery. A longitudinal study was performed at 2 and 4 weeks after surgery with **5**. **3** accumulated higher at 4 weeks after surgery (Fig. 14) and a significantly higher uptake was obtained at each time point studied in the aneurismal left carotid than in the control. Moreover the uptake of **3** was significantly correlated with MMP-2 and MMP-9 activity evaluated by zymography. Administration of a 50-fold excess of non-labelled precursor 15 minutes before **3** led to a significantly decreased uptake of **3** in the left carotid which was confirmed by autoradiography. Addition of 1,10-phenanthroline reduced substantially *ex vivo* binding of **3** in carotid aneurysm. Longitudinal study with **5** resulted in no significant correlation between retention of **5** and aneurysm size at 4 weeks; however the accumulation of **5** at 2 weeks substantially correlated with aneurysm size at 4 weeks. Although **5** gave a better quality image than **3**, no quantitative difference between both tracers was observed.

[<sup>111</sup>In]-RP782 **3** and [<sup>99m</sup>Tc]-(HYNIC-RP805)(tricine)(TPPTS) **5** have been rather well-characterized in vascular remodeling, atherosclerotic lesions and aneurysm. The observed target-to-nontarget ratios were acceptable for preclinical imaging. However, **3** and **5** were not tested in any tumor models, nor in models of inflammation such as asthma, COPD or rheumatoid arthritis.

#### Marimastat, 6a; Marimastat-FITC, 6b; Marimastat-ArB<sup>18</sup>F<sub>3</sub>, 6c; and control-ArBF<sub>3</sub> lacking the Marimastat moiety 6d

Keller *et al.* [40]; [41] tested two modified versions of the drug Marimastat ((2S,3R)-N4-[(1S)-2,2-dimethyl-1-[(methylamino)carbonyl]propyl]-N1,2-dihydroxy-3-(2-methylpropyl)butanedia-mide) **6a** (Fig. 6) in a cancer model. **6a** was transformed by addition of a linker in the S3' pocket which was either coupled with fluorescein isothiocyanate (FITC) leading to Marimastat-FITC **6b** (Fig. 6) or with an aryl boronic ester for one-step [<sup>18</sup>F]-aqueous fluoride capture leading to Marimastat-ArB<sup>18</sup>F<sub>3</sub> **6c** (Fig. 6). 67NR/CMV-luciferase murine mammary carcinoma xenograft mouse model was used for *in vivo* evaluation. Transcription of MMP-7, -13, -14 and -24 was significantly higher in controls than in tumors whereas MMP-2, -15, -23, -25 and -27 expression was higher in tumors compared to controls. **6a**, **6b** and Marimastat-ArBF<sub>3</sub> **6c** were tested in *in vitro* fluorogenic assays against MMP-2. They exhibited all IC<sub>50</sub> in the low nanomolar range (Table 3). Comparable studies of murine tissue lysates with **6b** indicated higher MMP activity in the tumors than in control mammary gland tissue. **6b** was tested in MDA-MB-231 cells transfected with human MMP-14 or empty vector followed by staining. Uptake of **6b** correlated with MMP-14 in MDA-MB-231 cells transfected with human MMP-14. The design of the *in vivo* experiment was the following: after 25 days of inoculation, a bioluminescent scan was performed which was followed the day after either by a PET scan with **6c** or control-ArBF<sub>3</sub> lacking the Marimastat moiety **6d** (Fig. 6). Specificity of **6c** was tested with injection of 300 nM **6a** (>10-fold excess of **6a**) 1 hour before tracer administration. Tumors were imaged by luciferase bioluminescence. The uptake of **6c** was low but detectable in the mammary carcinoma tumors while control-ArBF<sub>3</sub> **6d** did

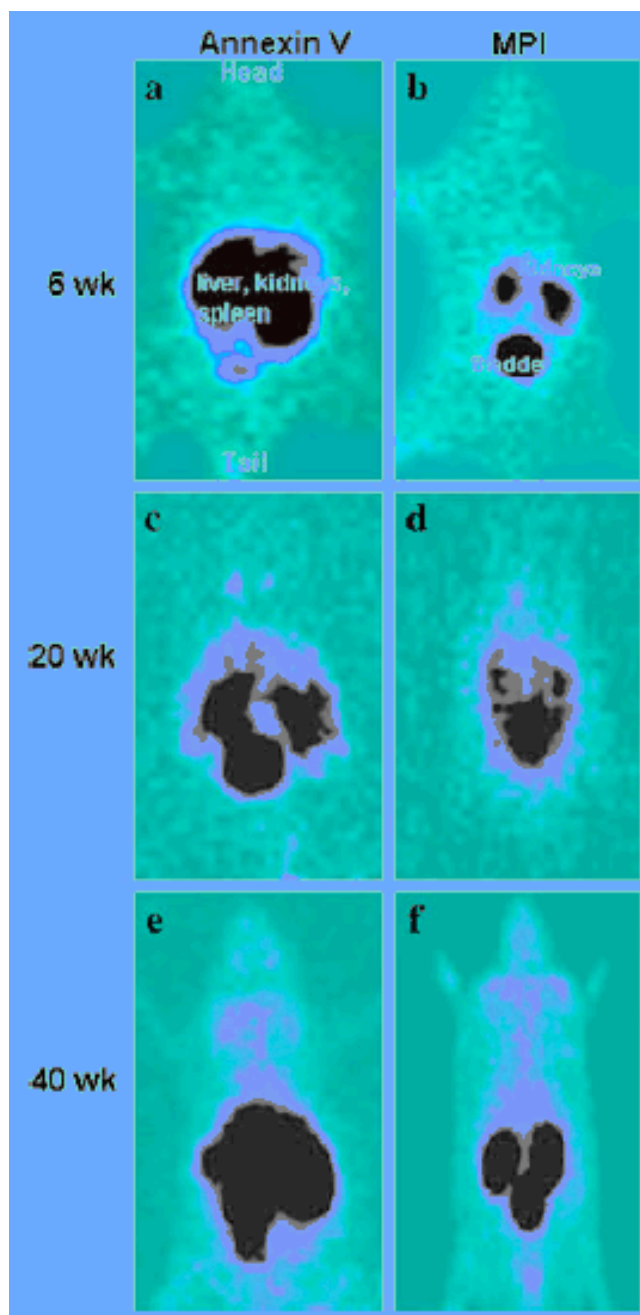


**Fig. (13).** *In vivo* antero-posterior images of apoE<sup>-/-</sup> mice injected with AA5 or 5 at three different time points.

not allow visualizing the tumor. The time activity curve indicated that a plateau level of radioactivity is reached in the tumor after 60 min. Blocking prior to tracer injection led to a decrease in retention of **6c** in the tumor (Fig. 15). To conclude, Marimastat was successfully radiolabelled with a novel [<sup>18</sup>F]-radiolabelling procedure in a low RCY. The newly obtained tracer Marimastat-ArB[<sup>18</sup>F]F<sub>3</sub> allowed specific visualization of 67NR tumor with a relatively low signal to noise ratio.

#### Nonpeptidomimetic Sulfonamide Hydroxamates

Nonpeptidomimetic MMPi were designed based on the three-dimensional structure of the MMP active site. These inhibitors, which bind in a non-covalent mode, all contain a sulfonyl group

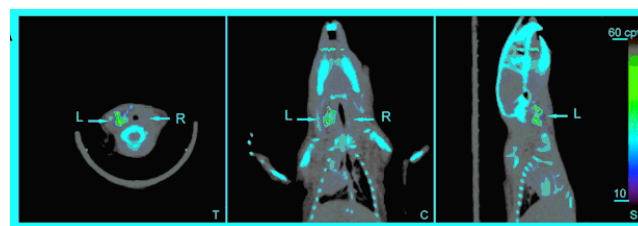


**Fig. (14).** Example of fused microSPECT/CT images of a mouse, 4 weeks after surgery inducing carotid aneurysm, after administration of **3**.

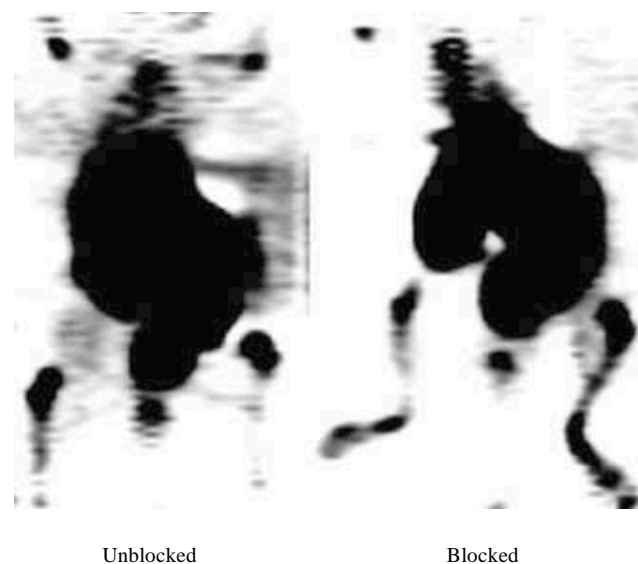


**Fig. (15).** *In vivo* microPET images of 67NR breast tumor mice injected with **6c** (left panel) and in a pre-blocked mouse (right panel) [40].

which affords hydrogen bonding with the enzymes. Because of their structure-based design, these compounds exhibit greater specificity than peptidomimetic compounds [13].

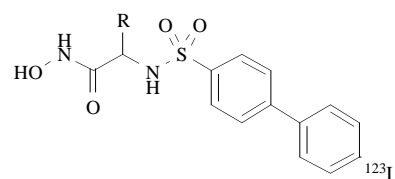
#### Biphenylsulfonamide Hydroxamate-based MMP Inhibitors

##### 2-(4'-[<sup>123</sup>I]iodo-biphenyl-4-sulfonylamino)-3-(1H-indol-3-yl)-propionamide, 7

Oltenfreiter *et al.* [42]; [43] synthesized the SPECT-tracer **7** (Fig. 16) by electrophilic aromatic substitution of the tributylstannyl derivative. *In vitro* fluorogenic assays were performed on the bromo and iodo inhibitors against pro-MMP-2, pro-MMP-9, the recombinant catalytic domain of MT1-MMP (cMT1) and MT3-MMP (cMT3). The bromo analog shows nanomolar affinities *in vitro* against pro-MMP-2, pro-MMP-9, cMT1 and cMT3 (Table 3). Inhibition values of the iodo inhibitor against pro-MMP-2, pro-MMP-9, cMT1 and cMT3 are also in the nanomolar range (Table 3). This radioiodinated tracer was evaluated in mice bearing A549 lung tumors. Tumor %ID/g was  $0.72 \pm 0.29$  3 hr p.i. and  $0.07 \pm 0.04$  48 hr p.i.; the tumors were not visualised at both time points. A tumor/blood ratio of 1.20 and a tumor/muscle ratio of 3.21 were obtained 48 hr p.i. The blood exhibited 66.2% of intact tracer whereas the tumor showed 87.8% of intact activity 2 hr p.i. However, metabolism and strong uptake in liver/intestines suggests that **7** is not a suitable tumor-imaging agent.

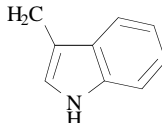
##### 2-(4'-[<sup>123</sup>I]iodo-biphenyl-4-sulfonylamino)-3-methylbutyramide, 8

Oltenfreiter *et al.* [44]; [45] prepared the analogue **8** of the previous SPECT-tracer **7** (Fig. 16) by adding an isopropyl group



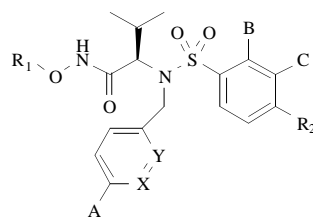
**R**

**7**



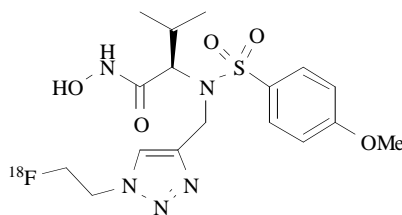
**8**

**CH(CH<sub>3</sub>)<sub>2</sub>**



	R <sub>1</sub>	A	X	Y	B	C	R <sub>2</sub>
<b>9</b>	H	H	CH	CH	H	H	O <sup>11</sup> CH <sub>3</sub>
<b>10</b>	<sup>11</sup> CH <sub>3</sub>	H	CH	CH	H	H	OMe
<b>11</b>	H	H	N.HCl	CH	H	H	OMe
<b>12a</b>	H	H	CH	CH	H	H	OCH <sub>2</sub> CH <sub>2</sub> <sup>18</sup> F
<b>12b</b>	H	H	CH	CH	H	H	<sup>18</sup> F
<b>13a</b>	<sup>11</sup> CH <sub>3</sub>	H	N	CH	H	H	OMe
<b>13b</b>	<sup>11</sup> CH <sub>3</sub>	H	CH	N	H	H	OMe
<b>13c</b>	<sup>11</sup> CH <sub>3</sub>	H	N	CH	NO <sub>2</sub>	H	H
<b>13d</b>	<sup>11</sup> CH <sub>3</sub>	H	N	CH	H	NO <sub>2</sub>	H
<b>13e</b>	<sup>11</sup> CH <sub>3</sub>	H	N	CH	H	H	NO <sub>2</sub>
<b>14a</b>	<sup>11</sup> CH <sub>3</sub>	H	N	CH	F	H	H
<b>14b</b>	<sup>11</sup> CH <sub>3</sub>	H	N	CH	H	H	F
<b>14c</b>	<sup>11</sup> CH <sub>3</sub>	H	N	CH	Cl	H	H
<b>14d</b>	<sup>11</sup> CH <sub>3</sub>	H	N	CH	H	Cl	H
<b>14e</b>	<sup>11</sup> CH <sub>3</sub>	H	N	CH	H	H	Cl
<b>14f</b>	<sup>11</sup> CH <sub>3</sub>	H	N	CH	Br	H	H
<b>14g</b>	<sup>11</sup> CH <sub>3</sub>	H	N	CH	H	Br	H
<b>14h</b>	<sup>11</sup> CH <sub>3</sub>	H	N	CH	H	H	Br
<b>14i</b>	<sup>11</sup> CH <sub>3</sub>	H	N	CH	H	H	I
<b>15a</b>	H	H	N	CH	H	I	OH
<b>15b</b>	H	H	N	CH	H	<sup>123</sup> I	OH
<b>15c</b>	H	H	N	CH	H	<sup>125</sup> I	OH
<b>15d</b>	H	H	N	CH	H	H	I
<b>15e</b>	H	H	N	CH	H	H	<sup>123</sup> I

15f	H	H	N	CH	H	H	<sup>125</sup> I
16	H	H	N	CH	H	H	OCH <sub>2</sub> CH <sub>2</sub> <sup>18</sup> F
17	H	<sup>18</sup> F	N	CH	H	H	OMe



18

Fig. (16). Structure of nonpeptidomimetic sulfonamide hydroxamate-based MMP inhibitors for PET/SPECT.

instead of a 1H-indol group at the alpha carbon of the hydroxamic acid. The iodo inhibitor was tested in *in vitro* fluorogenic assays against cMT1, cMT3, pro-MMP-2 and pro-MMP-9 (Table 3). The iodo inhibitor shows  $10^{-8}$  to  $10^{-6}$  M affinities against pro-MMP-2, pro-MMP-9, cMT1 and cMT3. This radioiodinated tracer was tested on an A549 adenocarcinoma xenograft mouse model. Tumors were slightly visualised in the scan and a low tumor uptake was obtained:  $0.71 \pm 0.08$  ID/g 3 hr p.i. and  $0.17 \pm 0.08$  ID/g 48 hr p.i. At 48 hr p.i., a tumor/blood ratio of 1.04 and a tumor/muscle ratio of 1.57 were obtained. Two third of intact tracer and one metabolite were found in the plasma whereas the tumor showed approximately 90% of intact tracer 2 hr p.i. Additional studies are necessary to show the specificity of the binding of **8**.

#### N-Benzene-benzenesulfonamide hydroxamate-based MMP inhibitors

##### [<sup>11</sup>C]-(*N*-hydroxy-(*R*)-2-[(4'-[<sup>11</sup>C] methoxyphenyl) sulfonyl]benzylamino)-3-methylbutanamide) - [<sup>11</sup>C]CGS 25966, **9**

Fei *et al.* [46] synthesized **9** (Fig. 16) by selective methylation of the phenol-hydroxyl group with [<sup>11</sup>C]-methyl triflate. Inhibition values against MMP-1, -2, -3, -8, -9 and -12 were in the nanomolar range (Table 3).

Zheng *et al.* [47] evaluated **9** in mice bearing MCF-7 (transfected with IL-1a) or MDA-MB-435 tumors (models of human breast cancer metastasis, which express MMP activity). At 45 minutes p.i., the %ID/g, tumor/ blood and tumor/ muscle ratios were respectively 0.42, 1.09 and 0.84 for MCF-7/IL-1a and 1.53, 1.27 and 1.95 for MDA-MB-435 tumors. Tumors were not visible in either of the tumor models, which suggest that **9** is not a suitable PET tracer for cancer imaging.

##### [<sup>11</sup>C]-Methyl-benzyl-CGS 25966, **10**

Fei *et al.* [48] performed [<sup>11</sup>C]-methylation of CGS 25966 at the aminohydroxyl position leading to the lipophilic inhibitor **10** (Fig. 16). As the ZBG of O-methylated hydroxamic acid has an identical role as the ZBG of hydroxamic acid, the structural modification of CGS 25966 to methylated CGS 25966 **10** was supposed not to alter its inhibitory property. A fibril degradation assay with fluorogenic substrates specific for MMP-1 was performed with **10** and CGS 27023A **11** (N-hydroxy-2(R)-[(4- methoxyphenyl)sulfonyl](3-picolyl)-amino]-3-methyl-butamide) (Fig. 16); [49]. **11** has a similar structure as CGS 25966 except the N-substituent was replaced by a picolyl group. **11** is a potent MMP inhibitor for several MMP subtypes [46]; (Table 3). Thus, the fibril degradation assay demonstrated that the modified compound **10** showed strong inhibitory effectiveness against MMP-1, compared to **11**.

##### [<sup>18</sup>F]-fluoroethoxy-CGS 25966 - [<sup>18</sup>F]-BR351, **12a**

A fluorinated MMP inhibitor **12a** (called [<sup>18</sup>F]-BR351) (Fig. 16) based on the broad-spectrum inhibitor CGS 25966 was prepared by Wagner *et al.* [50]; [51]. A fluorogenic assay on the reference

compound was performed. Measured inhibition constants are in the nanomolar range for MMP-2, -8, -9 and -13 (Table 3). [<sup>18</sup>F]-fluoroethoxy-CGS 25966 **12a** was tested in wild-type (WT) mice. *Ex vivo* analysis showed no tissue specific accumulation of **12a**. Blocking with unlabelled **12a** (10 min previous tracer injection) did not exhibit a significant effect on the biodistribution and clearance, thus no specific binding of **12a** to MMPs was observed in any tissues. Studies in cancer, inflammation, or atherosclerosis models have not yet been performed.

Toxicological tests [52] of the reference compound **12a** in rats were performed and no toxicity was observed when [<sup>19</sup>F]-**12a** was administered at the mg/kg-range to rats.

#### Picolyl-benzenesulfonamide Hydroxamate-based MMP Inhibitors

##### [<sup>11</sup>C]-methyl-CGS 27023A, **13a**; [<sup>11</sup>C]-methyl-2-picolyl-CGS 27023A, **13b**; [<sup>11</sup>C]-methyl-2-nitro-CGS 27023A, **13c**; [<sup>11</sup>C]-methyl-3-nitro-CGS 27023A, **13d**; and [<sup>11</sup>C]-methyl-4-nitro-CGS 27023A, **13e**

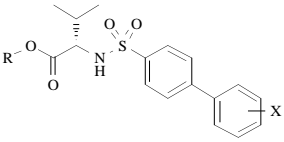
Fei *et al.* [48] prepared five analogs of CGS 27023A **11**: [<sup>11</sup>C]-methyl-CGS 27023A **13a**, [<sup>11</sup>C]-methyl-2-picolyl-CGS 27023A **13b**, [<sup>11</sup>C]-methyl-2-nitro-CGS 27023A **13c**, [<sup>11</sup>C]-methyl-3-nitro-CGS 27023A **13d** and [<sup>11</sup>C]-methyl-4-nitro-CGS 27023A **13e** (Fig. 16). Those five inhibitors were also tested in a fibril degradation assay against active MMP-1. It demonstrated substantial inhibitory effectiveness of these inhibitors similar to **11**, although the nitro-inhibitors displayed a slightly reduced inhibitory potency.

##### [<sup>11</sup>C]Me-2-F-CGS 27023A, **14a**; [<sup>11</sup>C]Me-4-F-CGS 27023A, **14b**; [<sup>11</sup>C]Me-2-Cl-CGS 27023A, **14c**; [<sup>11</sup>C]Me-3-Cl-CGS 27023A, **14d**; [<sup>11</sup>C]Me-4-Cl-CGS 27023A, **14e**; [<sup>11</sup>C]Me-2-Br-CGS 27023A, **14f**; [<sup>11</sup>C]Me-3-Br-CGS 27023A, **14g**; [<sup>11</sup>C]Me-4-Br-CGS 27023A, **14h**; and [<sup>11</sup>C]Me-4-I-CGS 27023A, **14i**

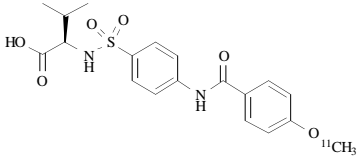
Zheng *et al.* [53] synthesized a library of [<sup>11</sup>C]methyl-halo-CGS 27023A analogs: [<sup>11</sup>C]Me-2-F-CGS 27023A **14a**, [<sup>11</sup>C]Me-4-F-CGS 27023A **14b**, [<sup>11</sup>C]Me-2-Cl-CGS 27023A **14c**, [<sup>11</sup>C]Me-3-Cl-CGS 27023A **14d**, [<sup>11</sup>C]Me-4-Cl-CGS 27023A **14e**, [<sup>11</sup>C]Me-2-Br-CGS 27023A **14f**, [<sup>11</sup>C]Me-3-Br-CGS 27023A **14g**, [<sup>11</sup>C]Me-4-Br-CGS 27023A **14h** and [<sup>11</sup>C]Me-4-I-CGS 27023A **14i** (Fig. 16). A fibril degradation assay with fluorogenic substrates specific to MMP-1 was performed with the reference compounds of these inhibitors **14a-i** and **9**. This library of inhibitors showed significant inhibitory effectiveness against MMP-1, similar to the parent compound CGS 27023A. No *in vivo* evaluation was performed.

##### [<sup>125</sup>I]-HO-CGS 27023A, **15a**; [<sup>125</sup>I]-HO-CGS 27023A, **15b**; [<sup>125</sup>I]-HO-CGS 27023A, **15c**; [<sup>125</sup>I]-CGS 27023A, **15d**; [<sup>125</sup>I]-CGS 27023A, **15e**; and [<sup>125</sup>I]-CGS 27023A, **15f**

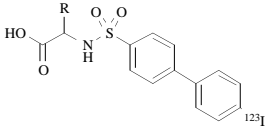
Kopka *et al.* [54] modified and radiolabelled CGS 27023A resulting in six iodo derivatives of **12**: I-HO-CGS 27023A **15a**, [<sup>125</sup>I]-HO-CGS 27023A **15b**, [<sup>125</sup>I]-HO-CGS 27023A **15c**, I-CGS

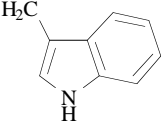


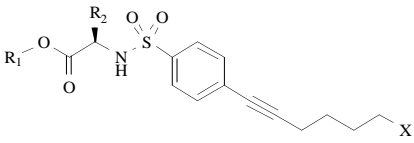
	R	X
19	H	O <sup>11</sup> CH <sub>3</sub>
20a	<sup>11</sup> CH <sub>3</sub>	2-OMe
20b	<sup>11</sup> CH <sub>3</sub>	3-OMe
20c	<sup>11</sup> CH <sub>3</sub>	4-OMe
20d	<sup>11</sup> CH <sub>3</sub>	2-F
20e	<sup>11</sup> CH <sub>3</sub>	3-F
20f	<sup>11</sup> CH <sub>3</sub>	4-F
20g	<sup>11</sup> CH <sub>3</sub>	4-NO <sub>2</sub>
21a	H	4-OMe
21b	H	4-F
21c	H	4-NO <sub>2</sub>

**22**



	R
23	
24	CH(CH <sub>3</sub> ) <sub>2</sub>

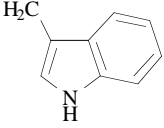
	R <sub>1</sub>	R <sub>2</sub>	X
25a	H	CH(CH <sub>3</sub> ) <sub>2</sub>	<sup>18</sup> F
25b	Me	CH(CH <sub>3</sub> ) <sub>2</sub>	<sup>18</sup> F
25c	H	(CH <sub>2</sub> ) <sub>2</sub> SCH <sub>3</sub>	<sup>18</sup> F
25d	H		<sup>18</sup> F
26	<sup>11</sup> CH <sub>3</sub>	CH(CH <sub>3</sub> ) <sub>2</sub>	<sup>19</sup> F

Fig. (17). Structure of carboxylate-based MMP inhibitors for PET/SPECT.

27023A **15d**, [<sup>123</sup>I]I-CGS 27023A **15e** and [<sup>125</sup>I]I-CGS 27023A **15f** (Fig. 16). *In vitro* studies indicated that **15d** has similar inhibitory potency as its parent compound **12** on the other hand **15a** showed decreased inhibitory effectiveness compared to **12** (Table 3) which is probably due to the strain of the polar hydroxyl group for entry into the hydrophobic S1' pocket supplemented by the steric hindrance of the bulky ortho iodine. An *in vivo* biodistribution study using **15c** in wild-type mice showed rapid blood and plasma clearance and low retention in normal tissues.

Schäfers *et al.* [55] evaluated **15e** four weeks after left carotid ligation and cholesterol-rich diet in apoE<sup>-/-</sup> mice, WT mice and sham-operated controls. [<sup>123</sup>I]I-HO-CGS 27023A accumulated progressively in the left carotid lesion of apoE<sup>-/-</sup> mice whereas neither carotid-ligated wild-type mice nor sham-operated apoE<sup>-/-</sup> mice exhibited any specific retention of **15e** in the region of interest. ApoE<sup>-/-</sup> mice with surgery have approximately 1.5 fold increase of **15e** in the left carotid ligation compared to apoE<sup>-/-</sup> mice injected with 1.2 μmol of CGS 27023A 2 hours before the scan. As vascular (carotid lesion) and paravascular accumulation of the radioligand can not be distinguished by planar scintigraphy, *ex vivo* analysis was performed to confirm the specificity of the binding. A 2.72-fold higher uptake in the left-carotid artery compared to the right-carotid artery was achieved. Moreover, after administration of 1.2 μmol of CGS 27023A, the uptake in left carotid artery was significantly reduced compared to the untreated left carotid artery (approximately 10 times) and no difference in the right-carotid artery between unblocked and blocked ApoE<sup>-/-</sup> mice was observed. Finally, microautoradiography with [<sup>125</sup>I]I-HO-CGS 27023A **15e** was performed in order to prove that binding of **15e** coincided with lesions that were rich in MMP activity. The autoradiographic signal in the carotid lesion matched with areas that were high in MMP-9 activity, confirmed by immunostaining. **15e** allowed detecting specifically MMP activity *in vivo* in the MMP-rich vascular lesions developed after carotid artery ligation and cholesterol-rich diet in apolipoprotein E-deficient mice.

#### **[<sup>18</sup>F]fluoroethoxy-CGS 27023A, 16**

Breyholz *et al.* [51]; [56] performed fluoroalkylation of the phenolic hydroxyl group of CGS 27023A in order to produce [<sup>18</sup>F]fluoroethoxy-CGS 27023A **16** (Fig. 16). Fluorogenic *in vitro* assays showed nanomolar affinities of [<sup>19</sup>F]fluoroethoxy-CGS 27023A against MMP-2, -8, -9 and -13 (Table 3). [<sup>18</sup>F]fluoroethoxy-CGS 27023A, **16** was only tested in WT mice and showed no tissue specific accumulation.

#### **[<sup>18</sup>F]CGS 27023A, 17**

Wagner *et al.* [50]; [57] synthesized **17** (Fig. 16), a fluorinated analog of CGS 27023A, by nucleophilic aromatic substitution of the corresponding bromide-precursor in one-step. **17** exhibited inhibitory potency in the low nanomolar range for MMP-2, -8, -9 and -13 (Table 3). Only a preliminary *in vivo* study in wild-type mice was performed, which indicated low background labelling in the healthy state.

#### **N-(Benzene-triazole)-benzenesulfonamide hydroxamate-based MMP inhibitors and N-triazole-benzenesulfonamide hydroxamate-based MMP inhibitors**

#### **(R)-2-(N-((1-(2-[<sup>18</sup>F]Fluoroethyl)-1H-1,2,3-triazol-4-yl)methyl)-4-methoxyphenylsulfonamido)-N-hydroxy-3-methylbutanamide, 18**

Hugenberg *et al.* [58] synthesized eight [<sup>19</sup>F]-fluorinated triazole-substituted hydroxamate MMPi and radiolabelled one of them **18** (Fig. 16). Fluorogenic inhibition assay of **18** against MMP-2, -8, -9 and -13 resulted in picomolar affinities (Table 3). The hydrophilic triazole nitrogen atoms could potentially give additional interactions with the Zn<sup>2+</sup> ion or other functional groups of the enzyme backbone. **18** exhibited excellent stability in human and mouse serum up to 120 min. **18** was tested in C57/Bl6 mice and did not exhibit any tracer specific accumulation. This MMPI was cleared rapidly and efficiently from the body through hepatic and

renal elimination. **18** was not tested in any animal model of pathologies.

### 2.2.2. Carboxylate-based MMP Inhibitors

Considering the importance of a ZBG for MMP inhibitors, compounds with other ZBGs have attracted large interest. The second most popular ZBG is the carboxylic acid moiety which interacts by mono-complexation with the zinc active site. It has been established that hydroxamate binding has a 3.5 kcal/mol advantage over carboxylate. The lower affinity is however counterbalanced by a superior metabolic stability [17].

#### Biphenylsulfonamide Carboxylate-based MMP Inhibitors

##### $[^{11}\text{C}]$ -(S)-2-(4'- $[^{11}\text{C}]$ methoxybiphenyl-4-sulfonylamino)-3-methylbutyric acid) - $[^{11}\text{C}]$ MSMA, **19**

Zheng *et al.* [47] prepared  $[^{11}\text{C}]$ MSMA **19** (Fig. 17) in a two step procedure by  $[^{11}\text{C}]$ -O-methylation of the benzyl ether precursor followed by a quick hydrolysis of the tert-butyl ester. MSMA showed nanomolar affinities for MMP-2, -3 and -13 and micromolar affinities for MMP-1, -7 and -9 (Table 3).  $[^{11}\text{C}]$ MSMA was tested in mice bearing breast cancer MCF-7 (transfected with IL-1a) or MDA-MB-435 tumors. At 45 minutes p.i., the %ID/g, tumor/blood and tumor/muscle ratios were 0.95, 0.99 and 1.21 for MCF-7/IL-1a xenograft and 0.98, 1.27 and 1.38 for MDA-MB-435 xenograft. None of the tumors were visible in a microPET scan, which suggests that **19** is not a suitable PET tracer for cancer imaging.

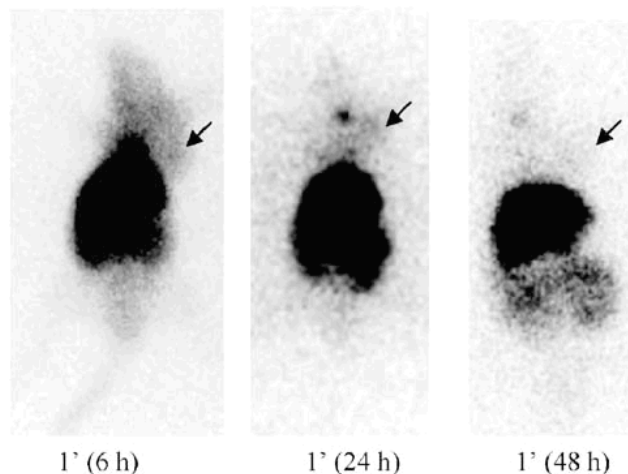


Fig. (18). Planar scintigraphy imaging of **24** at 6 hr, 24 hr and 48 hr p.i.

##### (S)-3-methyl-2-(2',3',4'-methoxybiphenyl-4-sulfonylamino) butyric acid $[^{11}\text{C}]$ methyl ester, **20a**, **20b**, **20c**; (S)-3-methyl-2-(2',3',4'-fluorobiphenyl-4-sulfonylamino)butyric acid $[^{11}\text{C}]$ methyl ester, **20d**, **20e**, **20f**; and (S)-3-methyl-2-(4'-nitrobiphenyl-4-sulfonylamino)butyric acid $[^{11}\text{C}]$ methyl ester, **20g**

Fei *et al.* [59] synthesized a series of seven MMP inhibitors by  $[^{11}\text{C}]$ -methylation of the corresponding carboxylate precursors: (S)-3-methyl-2-(2'-methoxybiphenyl-4-sulfonylamino)butyric acid  $[^{11}\text{C}]$ methyl ester, **20a**, (S)-3-methyl-2-(3'-methoxybiphenyl-4-sulfonylamino)butyric acid  $[^{11}\text{C}]$ methyl ester, **20b**, (S)-3-methyl-2-(4'-methoxybiphenyl-4-sulfonylamino)butyric acid  $[^{11}\text{C}]$ methyl ester, **20c**, (S)-3-methyl-2-(2'-fluorobiphenyl-4-sulfonylamino)butyric acid  $[^{11}\text{C}]$ methyl ester, **20d**, (S)-3-methyl-2-(3'-fluorobiphenyl-4-sulfonylamino)butyric acid  $[^{11}\text{C}]$ methyl ester, **20e**, (S)-3-methyl-2-(4'-fluorobiphenyl-4-sulfonylamino)butyric acid  $[^{11}\text{C}]$ methyl ester, **20f**, and (S)-3-methyl-2-(4'-nitrobiphenyl-4-sulfonylamino)butyric acid  $[^{11}\text{C}]$ methyl ester **20g** (Fig. 17). The corresponding carboxylic acids of **20c**, **20f** and **20g** are **21a**, **21b** and **21c** (Fig. 17). The reference compounds of **20a-g** and **21a-c** were tested in a fibril degrada-

tion assay with fluorogenic substrates specific for active MMP-13. This library of inhibitors showed significant inhibitory effectiveness against MMP-13. Fei *et al.* preferred to make the  $[^{11}\text{C}]$ -labeled methyl ester prodrug (neutral) rather than the  $[^{11}\text{C}]$ -labeled acid drug (positively charged at physiological pH) because of the easier synthesis of the methyl ester prodrug compared to the parent carboxylic acid drug. Furthermore, the methyl ester is equivalent to carboxylic acid in binding zinc in SAR study [11]. None of the compounds **20a-g** was tested *in vivo*.

##### (2R)-3-methyl-2-[[4-(4- $[^{11}\text{C}]$ methoxybenzoyl)amino]benzenesulfonyl]amino]butanoic acid, **22**

Kuhnast *et al.* [60] prepared (2R)-3-methyl-2-[[4-(4- $[^{11}\text{C}]$ methoxybenzoyl)amino]benzenesulfonyl] amino]butanoic acid **22** (Fig. 17) by methylation of the phenol precursor. An *in vitro* gelatin degradation assay on the reference compound was performed and sub-micromolar  $\text{IC}_{50}$  values were obtained (Table 3). Biodistribution and *in vivo* serum stability tests in normal mice were carried out. **22** showed rapid excretion within the first 30 min after injection. In addition, **2** exhibited stability towards degradation up to 30 min p.i.

##### 2-(4'- $[^{123}\text{I}]$ iodo-biphenyl-4-sulfonylamino)-3-(1H-indol-3-yl)-propionic acid, **23**

Oltenfreiter *et al.* [42]; [43] prepared the highly lipophilic tracer 2-(4'- $[^{123}\text{I}]$ iodo-biphenyl-4-sulfonylamino)-3-(1H-indol-3-yl)-propionic acid **23** (Fig. 17). The corresponding bromo and iodo inhibitors were tested in *in vitro* fluorogenic assays against recombinant pro-MMP-2, pro-MMP-9, cMT1 and cMT3. They exhibited affinities in the  $10^{-9}$  to  $10^{-7}$  M range for the bromo-inhibitor and the iodo-inhibitor (Table 3). **23** was evaluated in mice bearing A549 lung tumors. Tumor ID/g were  $0.27 \pm 0.10$  at 3 hr p.i. and  $0.04 \pm 0.05$  at 48 hr p.i. but the tumors were not visualised at both time points. A tumor/blood ratio of 3.09 and a tumor/muscle ratio of 0.8 were obtained 48 hr p.i. 5% of intact tracer was found in the blood while the tumor exhibited 75.9% of intact activity at 2 hr p.i. The rather negative outcome of this study (low tumor uptake, high metabolism, high uptake in liver/intestines) suggests that **23** is not a suitable tumor-imaging agent.

##### 2-(4'- $[^{123}\text{I}]$ iodo-biphenyl-4-sulphonylamino)-3-methyl-butylric acid, **24**

Oltenfreiter *et al.* [44]; [45] synthesized the SPECT-tracer 2-(4'- $[^{123}\text{I}]$ iodo-biphenyl-4-sulphonylamino)-3-methyl-butylric acid **24** (Fig. 17). The reference compound showed  $10^{-8}$  to  $10^{-7}$  M affinities against pro-MMP-2, pro-MMP-9, cMT1 and cMT3 (Table 3). **24** was tested in a A549 xenograft mouse model. A low tumor uptake was found, tumors were faintly visualised in the scan (Fig. 18). Tumor uptake was  $2.00 \pm 0.40$  ID/g at 3 hr p.i. and  $0.75 \pm 0.44$  ID/g at 48 hr p.i. A tumor/blood ratio of 0.52 and a tumor/muscle ratio of 4.63 were obtained at 48 hr p.i. Metabolite analysis showed hardly any degradation of **24** at 2h p.i. Image quality was improved by decreasing the specific activity of **24** leading to a lower liver uptake due to saturable binding in the liver. Further analysis is required to prove the specificity of the binding of **24**.

#### Phenylsulfonamide carboxylate-based MMP inhibitors with a linear side chain

##### (2R)-2-[4-(6- $[^{18}\text{F}]$ fluorohex-1-ynyl)benzene-sulfonylamino]-3-methylbutyric acid - $[^{18}\text{F}]$ SAV03, **25a**

Furumoto *et al.* [61] prepared **25a** (called  $[^{18}\text{F}]$ SAV03) (Fig. 17) in one-pot synthesis by radiofluorination of the tosyl precursor followed by hydrolysis of the methyl ester. The reference compound showed micromolar affinity against MMP-2 (Table 3). A biodistribution study of **25a** using Ehrlich tumor bearing mice showed that uptake in tumor was higher than in other organs, except for the liver, small intestine and bone with %ID/g of  $0.52 \pm 0.16$  at 30 min and  $0.22 \pm 0.07$  at 120 min. Tumor/muscle and tu-



mor/blood ratios were  $2.31 \pm 1.09$  and  $8.42 \pm 3.31$  at 120 min respectively.

**(2R)-2-[4-(6- $^{18}$ F]Fluorohex-1-ynyl)benzene-sulfonylamino]-3-methylbutyric acid methyl ester -  $^{18}$ F]SAV03M, 25b**

Furumoto *et al.* [61] prepared also the methyl ester of **25a**, **25b** (Fig. 17) (called [ $^{18}$ F]SAV03M), in the same way as **25a** without the deprotection step. A comparative *in vivo* study by using **25b** as a prodrug was performed. The uptake in the liver at 30 min p.i. decreased by half and that in tumor increased by 2.4 times compared with **25a**. The tumor/muscle ratio was also much higher  $13.9 \pm 4.9$ , 120 min p.i. Radio-thin-layer chromatographic analysis of **25b** metabolites indicated that **25b** was easily converted to the parent drug **25a** *in vivo* and accumulated in tumor tissue. Specificity studies, such as pre-blocking mice or coinjection of unlabelled precursor, should be performed in order to check if **25b** is suitable for tumor imaging with PET.

**(2R)-2-[4-(6- $^{18}$ F]Fluorohex-1-ynyl)phenyl[sulfonylamino]-3-(1H-indol-3yl)propionic acid, 25c; and (2R)-2-[4-(6- $^{18}$ F]fluorohex-1-ynyl)phenyl[sulfonylamino]-3-methylbutyric acid, 25d**

Furumoto *et al.* [62] prepared two [ $^{18}$ F]-labeled MMP inhibitors **25c** and **25d** (Fig. 17) by variation of the substituents in  $\alpha$  of the carboxylic acid. No *in vitro* or *in vivo* studies were performed.

**(2R)-2-[4-(6-fluorohex-1-ynyl)phenyl[sulfonylamino]-3-methylbutyric acid [ $^{11}$ C]methyl ester -  $^{11}$ C]FMAME, 26**

Zheng *et al.* [63] prepared the methyl ester prodrug **26** (Fig. 17). The reference compound was also prepared. The parent drug FMA exhibited an  $IC_{50}$  of 1.9  $\mu$ M for MMP-2. This [ $^{11}$ C]-methyl ester prodrug was tested in mice bearing MCF-7/IL-1a or MDA-MB-435 tumors. Biodistribution at 30 min p.i. revealed a %ID/g, tumor/muscle and tumor/blood ratio of 1.13,  $1.05 \pm 0.29$  and  $0.77 \pm 0.20$  for MCF-7/IL-1a tumors and 1.37,  $0.99 \pm 0.35$  and  $1.44 \pm 0.69$  for MDA-MB-435 tumors. Pretreatment with 2.5 mg/kg of FMA 30 minutes before **26** administration did not lead to significant reduction of %ID/g, tumor/muscle and tumor/blood ratios for MCF-7/IL-1a and MDA-MB-435 tumors. The tumors were visualized in the PET scan but tracer binding was non-specific suggesting that **26** is not a suitable PET-tracer for tumor imaging.

### 2.2.3. Barbiturate-based MMP Inhibitors

Besides hydroxamates and carboxylates, another ZBG was tested for molecular imaging of metalloproteinase expression: pyrimidine-2,4,6-trione also named barbiturate. This novel ZBG (Fig. 19); [64] required a cyclic urea which coordinates the zinc monodentately via its carbonyl. One of the N-H groups from the urea is necessary for hydrogen bonding with Gly amide carbonyl and the other N-H required a low  $pK_a$  for hydrogen bonding to glutamate base. In addition, a linker which conformationally makes a U-turn between the ZBG and the P1' pocket is necessary. The linker must have an H-bond acceptor for interaction with Gly and Leu amide N-H. Finally, the P1' substituent should match the S1' pocket.

**5-[4-(2-Hydroxy-ethyl)-piperazin-1-yl]-5-[4-(4- $^{125}$ I]iodo-phenoxy)-phenyl]-pyrimidine-2,4,6-trione, 27**

Breyholz *et al.* [65] prepared a series of C-5-disubstituted barbiturate MMP inhibitors from which they only labelled one inhibitor with [ $^{125}$ I]NaI from the bromo-precursor to obtain **27** (Fig. 20). MMP-2 and MMP-9 fluorogenic assays on the nonradioactive reference compound were performed and low nanomolar values were obtained (Table 3). No *in vivo* studies have been performed.

**5-[4-(2- $^{18}$ F]Fluoroethyl)piperazin-1-yl]-5-(4-phenoxyphenyl)pyrimidine-2,4,6-trione, 28**

Breyholz *et al.* [66] radiosynthesized a [ $^{18}$ F]-fluoroethyl radioligand **28** (Fig. 20) in a two-step procedure. **28** has only been tested

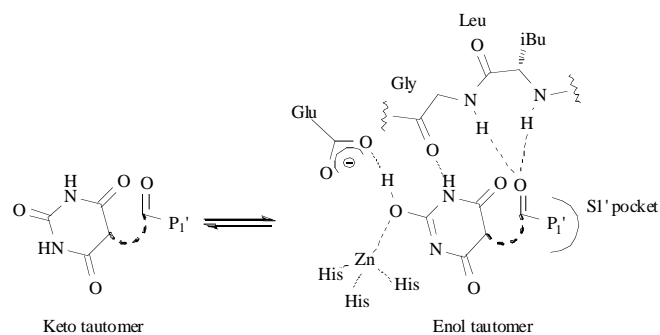


Fig. (19). Binding pose of the barbiturate ZBG into the active site of MMPs.

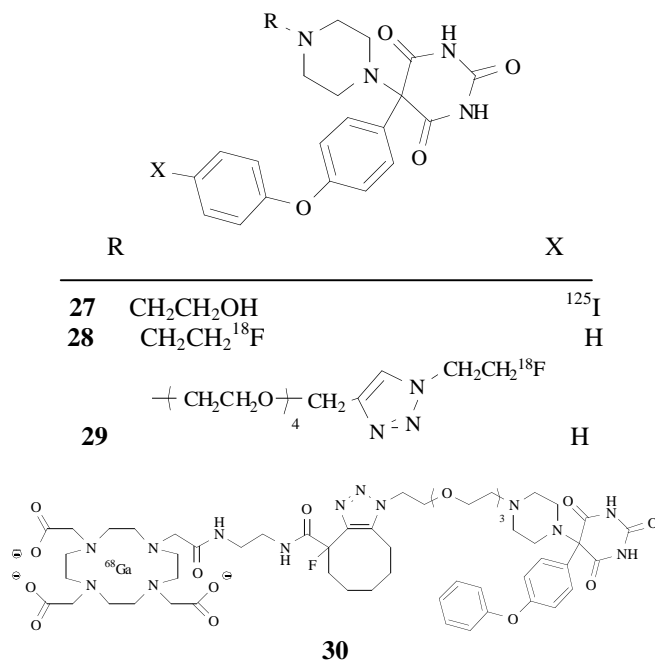


Fig. (20). Structure of barbiturate-based MMP inhibitors for PET/SPECT.

in wild-type mice and preliminary biodistribution studies showed no tissue specific accumulation with a predominantly renal excretion.

**5-(4-[2-[2-(2-[2-(2- $^{18}$ F]fluoroethyl)-1H-1,2,3-triazol-4-ylmethoxy]-ethoxy]-ethoxy]-ethyl)-piperazin-1-yl)-5-(4-phenoxyphenyl)-pyrimidine-2,4,6-trione, 29**

Schrigten *et al.* [67] prepared a library of barbituric acid-based MMP inhibitors of the second generation (less lipophilic). **29** (Fig. 20) was radiolabelled in a two-step procedure by fluorination of the tosyl-ethylazide followed by copper(I) catalyzed 1,3-dipolar cycloaddition. Fluorogenic inhibition assay of **29** against MMP-2, -8, -9 and -13 resulted in nanomolar affinities (Table 3). *In vitro* stability of this tracer in human serum for up to 120 min at 37°C was excellent. *In vivo* evaluation in WT mice demonstrated no tissue specific retention of **29** with a more rapid clearance behaviour of **29** compared to **28**.

**[ $^{68}$ Ga]-2,2',2''-(10-(2-(2-(4-fluoro-1-(2-(2-(2-(4-(2,4,6-trioxo-5-(4-phenoxyphenyl)hexahydropyrimidin-5-yl)piperazin-1-yl)ethoxy)ethoxy)ethoxy)ethyl)-4,5,6,7,8,9-hexahydro-1H-cycloocta[d][1,2,3]triazole-4-carboxamido)ethyl)amino)-2-oxoethyl)-1,4,7,10-tetraazacyclododecane-1,4,7-triyl)triacetate, 30**

Claesener *et al.* [68] prepared the PET-tracer **30** (Fig. 20) by copper-free cycloaddition of an azido moiety linked to the inhibitor

backbone and a cyclooctyne-DOTA derivative. **30** was radiolabelled with  $^{68}\text{Ga}$  and was radiosynthesized in two manners, either by a pre-labelling approach or a post-labelling one. The azido-precursor showed nanomolar affinities for the gelatinases: 24 nM for MMP-2 and 68 nM for MMP-9. No *in vitro* or *in vivo* studies were performed on **30**.

### 2.3. MMP Peptides

Peptides [69] were also developed as probes for non-invasive detection of MMP expression. Koivunen *et al.* prepared a specific gelatinase inhibitor from phage display peptide library: CTTHWGFTLC (Cys-Thr-Thr-His-Trp-Gly-Phe-Thr-Leu-Cys) **31** (abbreviated CTT) (Fig. 21). This cyclic decapeptide, which contains the motif *HWGF*, inhibited only gelatinases ( $\text{IC}_{50}$  (MMP-2) = 10  $\mu\text{M}$ ,  $\text{IC}_{50}$  (MMP-9) < 10  $\mu\text{M}$ ) whereas no inhibition was obtained for MMP-8, -13 and -14. Even if the inhibitory mechanism of this peptide is still unclear, the tryptophan residue fits probably the S1' pocket whereas the histidine residue could act as a ligand for the catalytic zinc ion. The cyclic conformation is essential for the activity of the peptide. CTTHWGFTLC was found to inhibit the migration of human endothelial cells and tumor cells. It also showed potent antitumor activity.

#### $^{125}\text{I}$ -yCTTHWGFTLC, 32

Kuhnast *et al.* [70] modified the N-terminal of **31** with a D-tyrosine and labeled the resulting peptide with  $^{125}\text{I}$ NaI in order to obtain  $^{125}\text{I}$ -yCTTHWGFTLC **32** (Fig. 21). yCTTHWGFTLC inhibited MMP-2 in the range of 5 to 10  $\mu\text{M}$  and the  $\text{IC}_{50}$  of MMP-9 was more than 10-fold lower (Table 3). Derivatisation of CTT did not affect its inhibitory properties towards gelatinases. After 60 min of incubation with the purified activated enzymes MMP-2 and MMP-9, the entire radioactivity was recovered as the intact tracer. **32** was tested in Lewis Lung cancer tumor bearing mice. Excretion organs (liver, kidneys and intestines) show high uptake and a moderate accumulation of **32** was obtained in the tumor. The tumor/muscle ratio was 2.56 at 2 hrs after injection. Metabolite analysis of the serum collected 10 min after injection indicated 75% of intact tracer with two metabolites, one of which is 3- $^{125}\text{I}$ iodo-D-tyrosine. Coinjection of 12 mg/kg of unlabelled peptide with **32** led to a significant decrease (37%) in tumor uptake, however treatment with yCTTHWGFTLC did not substantially affect the concentration of **32** in the blood. The poor metabolic stability and the small amount of specific binding of **32** make it unsuitable for targeting of gelatinases *in vivo*.

#### $^{64}\text{Cu}$ -DOTA-CTT, 33; and $^{64}\text{Cu}$ -DOTA-STT, 34

Sprague *et al.* [71] prepared a PET tracer from **31** by conjugation with the bifunctional chelator DOTA (1,4,7,10-tetraazacyclotetradecane-N,N',N'',N'''-tetraacetic acid) for radiolabelling with  $^{64}\text{Cu}$  leading to **33** (Fig. 21). The linearly scrambled peptide STTGHFWTLS (Ser-Thr-Thr-Gly-His-Phe-Trp-Thr-Leu-Ser) (abbreviated STT), which was used as a negative control, was also radiolabelled to give  $^{64}\text{Cu}$ -DOTA-STT **34** (Fig. 21). **33** and **34** were tested for *in vitro* stability with rat serum. After 1 hr of incubation, both tracers did not show any degradation. From 1 to 6 hr, more than 95% of the recovered radioactivity corresponded to **33**. Nevertheless, after 24hrs of incubation, the stability of **33** decreased substantially with 41.7  $\pm$  8.1% of intact tracer. Fluorogenic substrate assays of CTT, Cu(II)-DOTA-CTT, STT and Cu(II)-DOTA-STT were performed against human MMP-2 (hMMP-2), mouse MMP-9 (mMMP-9) and human MMP-9 (hMMP-9). Cu(II)-DOTA-CTT exhibited low micromolar affinities (Table 3). The conjugation of CTT to Cu(II)-DOTA did not substantially modify the affinity of the ligand towards the gelatinases. STT showed  $\text{EC}_{50}$  of >1000  $\mu\text{M}$ , 104  $\mu\text{M}$  and not determined (ND) and Cu(II)-DOTA-STT: >1000  $\mu\text{M}$ , 20.4  $\mu\text{M}$  and ND, respectively. STT has an affinity 10-fold lower than CTT for mMMP-9 however Cu(II)-DOTA-STT and Cu(II)-DOTA-CTT inhibited mMMP-9 in the same range. Neither STT nor Cu(II)-

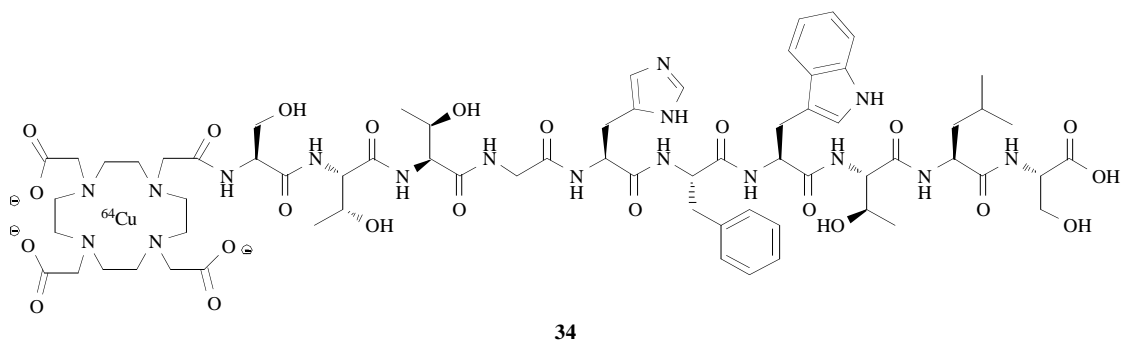
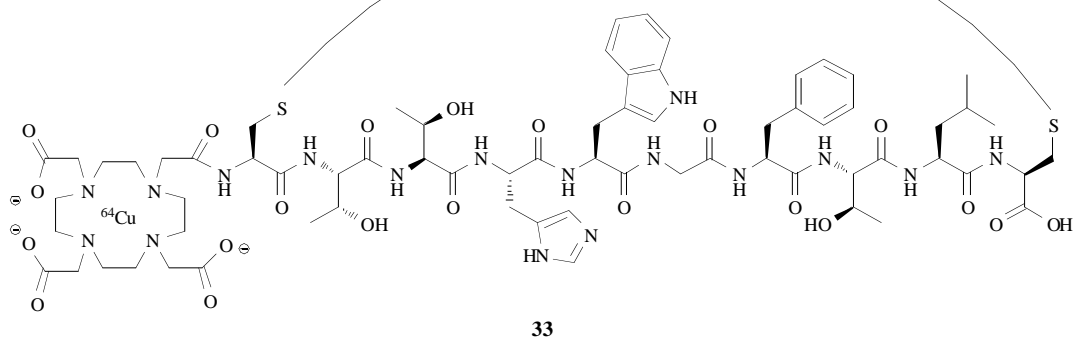
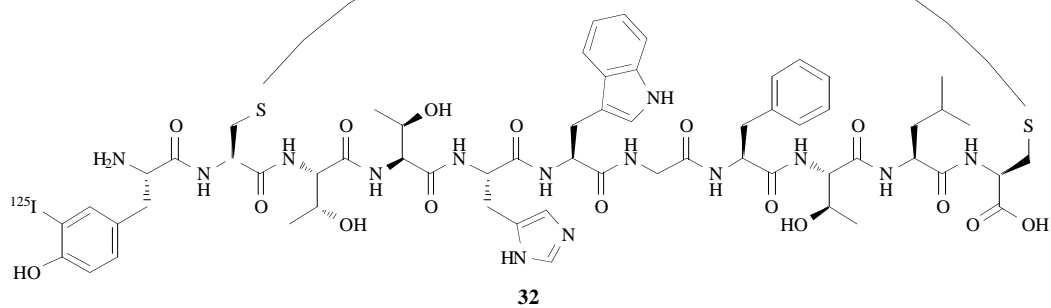
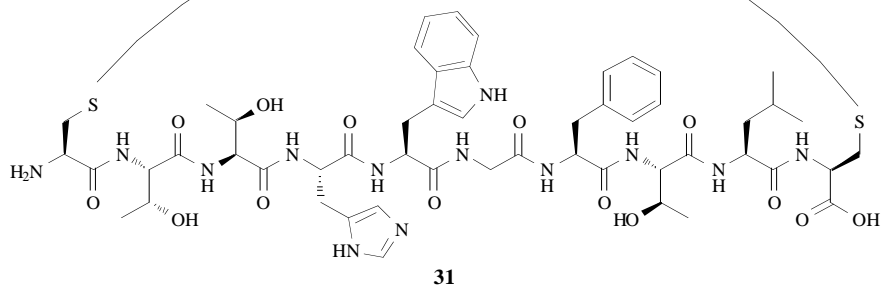
DOTA-STT inhibited hMMP-2. **33** and **34** were tested in B16F10 tumor-bearing mice. *Ex vivo* analysis demonstrated a 2.7-fold higher uptake in the tumor for **33** than **34** ( $2.44 \pm 0.26$  vs  $0.91 \pm 0.10$ ). However,  $^{64}\text{Cu}$ -DOTA-CTT showed higher accumulation in every organ than  $^{64}\text{Cu}$ -DOTA-STT. The tumor/blood ratio of **33** and **34** was not significantly different ( $2.12 \pm 0.70$  vs  $1.82 \pm 0.68$ ). MicroPET images also exhibited a two-fold higher uptake of **33** over **34**. Zymography indicated MMP-2 and MMP-9 expression in B16F10 tumor extracts and to a lower extent in blood. **33** and **34** were evaluated in a second tumor model: MDA-MB-435 tumor-bearing mice. Zymography demonstrated that the expression of both gelatinases was not consistent among the evaluated tumors evaluated and only one out of 24 scanned mice exhibited retention of **34** in MDA-MB-435 tumor, which was confirmed by zymography. Micromolar affinities towards the gelatinases and poor *in vivo* stability indicated that  $^{64}\text{Cu}$ -DOTA-STT is not a suitable radioligand for *in vivo* tumor imaging.

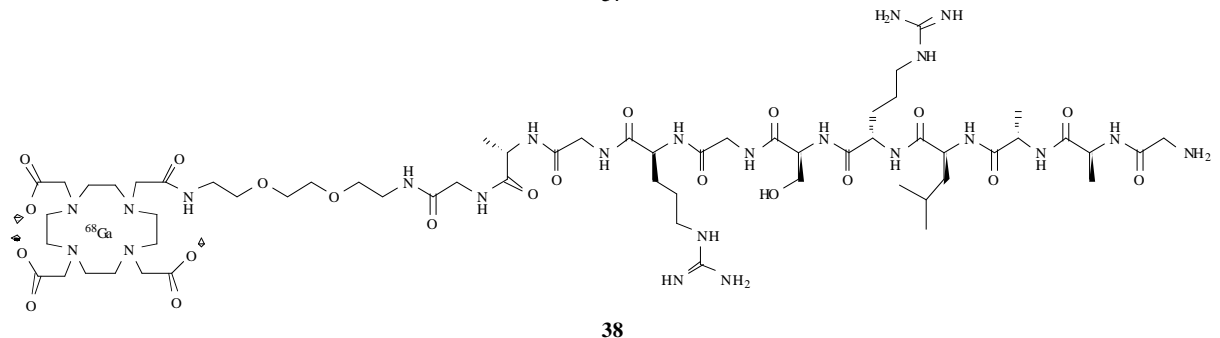
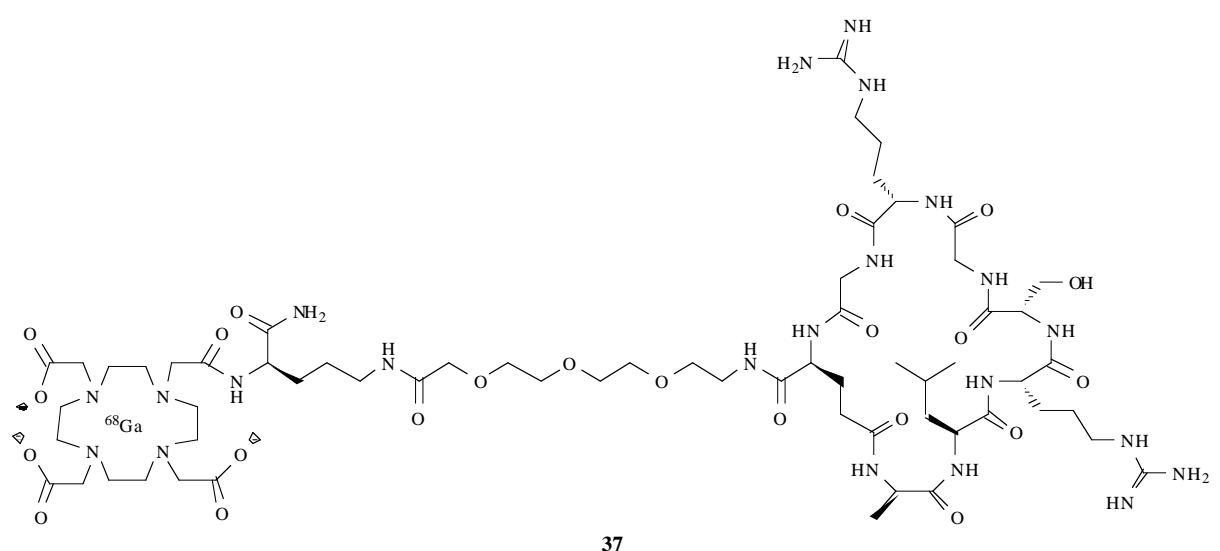
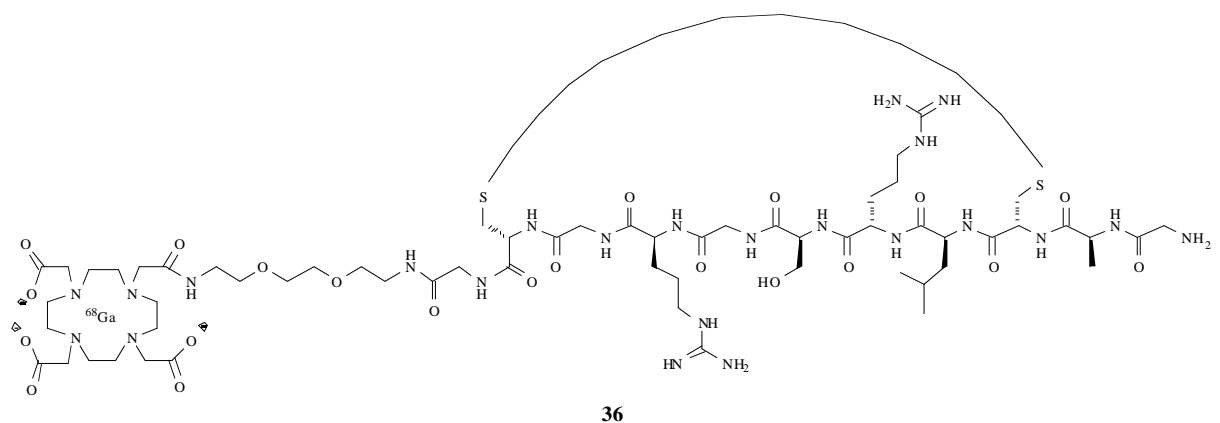
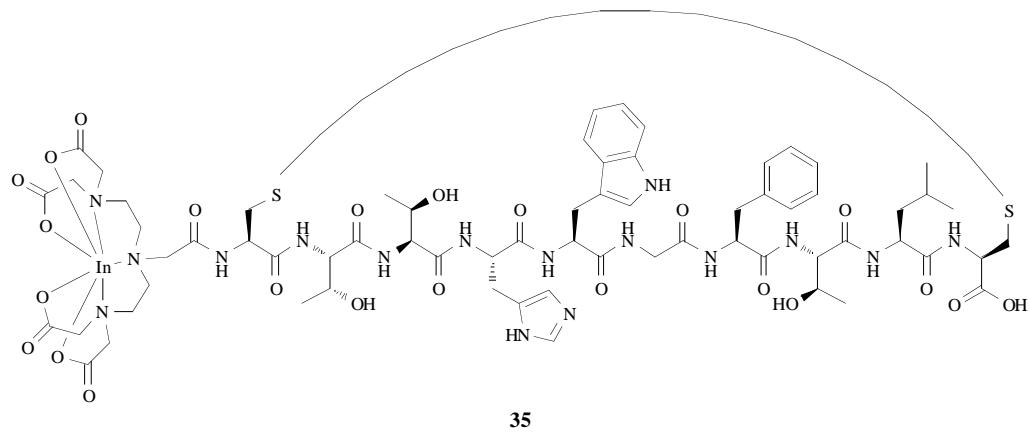
#### $^{111}\text{In}$ -DTPA-CTT, 35

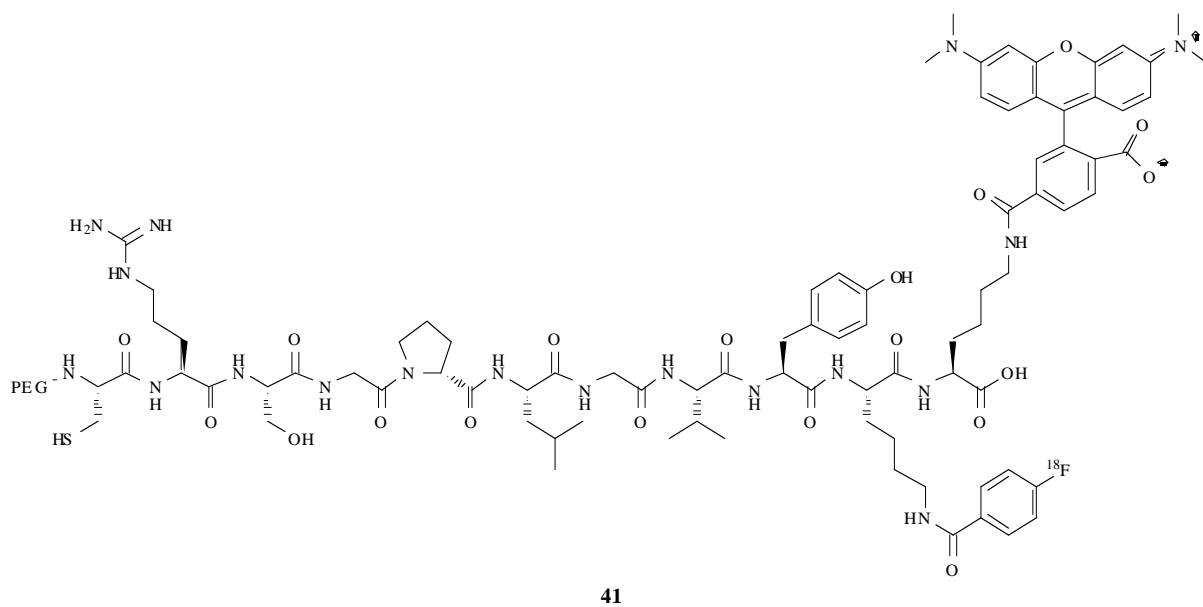
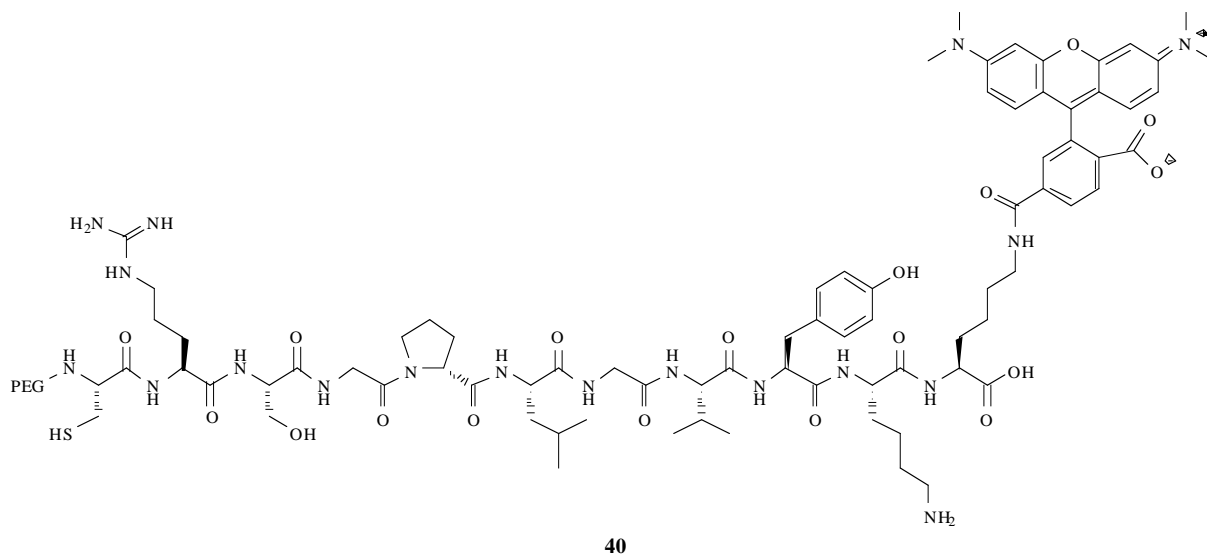
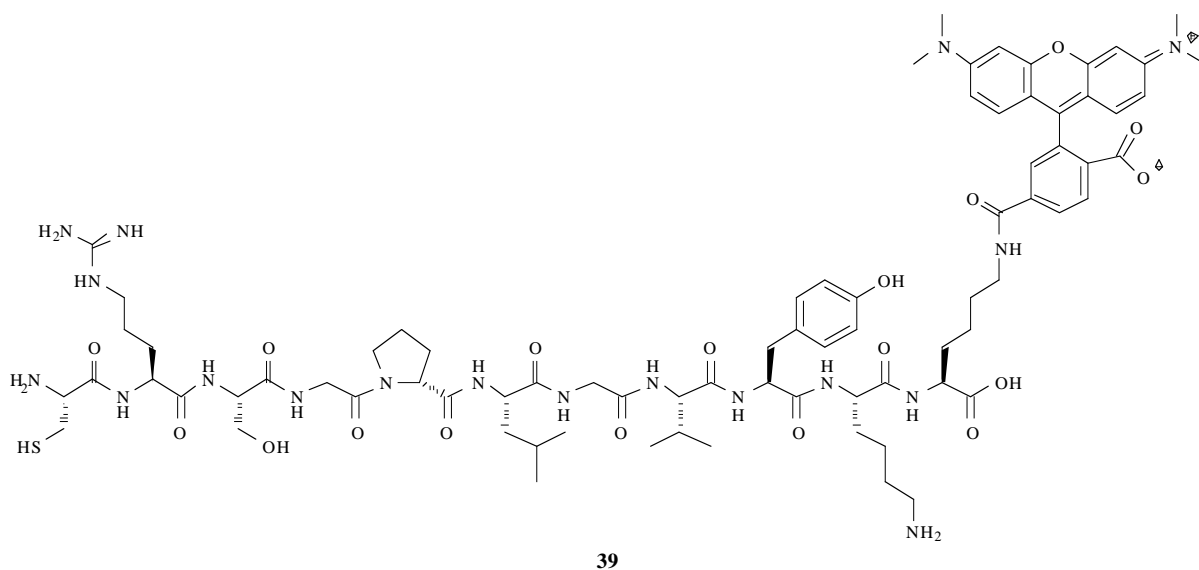
Hanaoka *et al.* [72] attached the highly hydrophilic and negatively charged  $^{111}\text{In}$ -DTPA to **31** in order to obtain  $^{111}\text{In}$ -DTPA-CTT **35** (Fig. 21). **35** exhibited lower  $\text{IC}_{50}$  than the mother compound CTT (Table 3). After 3 hrs of incubation at 37°C in murine serum, approximately 85% of the radioactivity represented intact tracer. **35** was tested in two xenograft mouse models: MDA-MB-231 and MDA-MB-435S. The % ID/g in the tumor 3 hr p.i. was higher in MDA-MB-231 xenograft than MDA-MB-435S xenograft. However the gelatinase activity was significantly stronger in MDA-MB-231 tumor than MDA-MB-435S tumor. The % ID/g in the tumor and the tumor-to-blood ratio demonstrated a substantial correlation with the amount of gelatinases, 0.735 and 0.801 respectively.

#### $^{68}\text{Ga}$ -DOTA-PEG(3)-GCGRGSRLCAG, 36; $^{68}\text{Ga}$ -(2-N-DOTA)-NH<sub>2</sub>- $\delta$ -D-Orn-(11-amino-3,6,9-trioxaundecanoyl)-ALRSGRGQ, 37; and $^{68}\text{Ga}$ -DOTA-PEG(3)-GAALRSGRGAG, 38

Ujula *et al.* [73] evaluated a MMP-9 targeting peptide obtained from a phage display (by biopanning of tumor cells) and two modified versions in a C8161T/M1 melanoma xenograft rat model. All three peptides were conjugated with DOTA and radiolabelled with  $^{68}\text{Ga}$  to lead to **36**, **37** and **38** (Fig. 21). All three PET peptides were stable in saline up to 4 hr. **37** did not show any degradation after 4 hr of incubation in human plasma; however **36** and **38** exhibited lower stability, with a respective half-life of about 2.5 hr and 1 hr. The plasma protein of **36** was analyzed *in vitro* and resulted in about 35  $\pm$  1% of the tracer complexed with plasma proteins. The stability of the peptides at 15 min and at 120 min p.i. was evaluated *in vivo* in a rat melanoma xenograft model in plasma, tumor and urine. It was shown that **37** exhibited the greatest stability *in vivo*, followed by **36**, in contrast to **38** which showed a fast degradation *in vivo*. **36** and **37** allowed visualizing clearly the tumor in the PET scan. **37** exhibited slower uptake in the tumor than **36**, however a longer retention in the tumor was observed due to the higher stability of the peptide. **38** showed an overall background signal. The tumor/muscle ratios after 120 min of administration of **36**, **37** and **38** were respectively  $5.5 \pm 1.3$ ,  $3.2 \pm 0.2$  and  $3.2 \pm 0.6$ . **36** demonstrated a tumor/blood ratio of  $1.2 \pm 0.3$  120 min p.i. *Ex vivo* biodistribution was performed on rats, after tumor growth from two to four weeks, administered with **36**. The highest SUV and tumor/muscle ratios were obtained three weeks after inoculation. Attempts to correlate MMP-9 levels by zymography with *ex vivo* data led to a weak correlation coefficient of 0.33. The parental compound **36** gave the highest retention in tumor. Even if the accumulation of **36** was low, additional studies have to be performed to prove its specificity. Modification of the peptide by a lactam bridge instead of a cystine bridge resulted in higher stability and should be further evaluated.







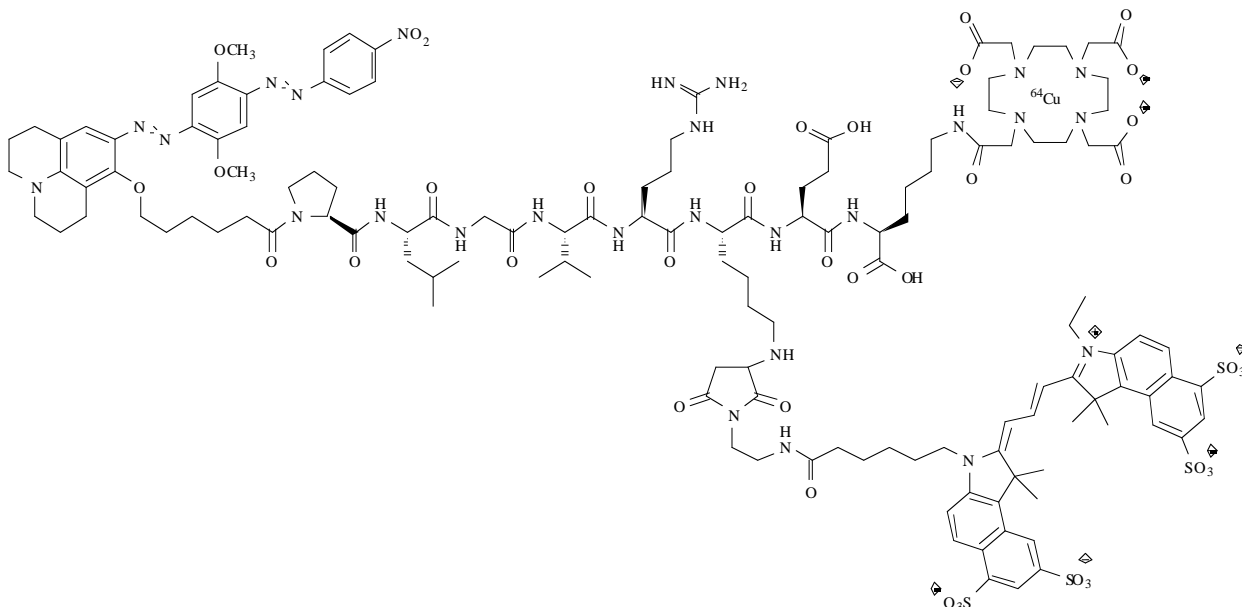


Fig. (21). Structure of MMP peptides for PET/SPECT.

**CRSGPLGVYKK-TMR, 39; PEG-CRSGPLGVYKK-TMR, 40; and PEG-[<sup>18</sup>F]-CRSGPLGVYKK-TMR, 41**

Cheng *et al.* [74] prepared three probes from the hydrophilic peptide Cys-Arg-Ser-Gly-Pro-Leu-Gly-Val-Thr-Lys-Lys (abbreviated CRSGLGVYKK) to which was attached the hydrophobic fluorescent dye tetramethylrhodamine (TMR) leading to **39**, **40** and **41** (Fig. 21). **39** was cleaved by purified MMP-2 or medium from HT1080 cells (MMP>0) to release TMR but not from MCF-7 cells (control). The cleavage of **39** was blocked by 10  $\mu$ M 1,10-phenanthroline which demonstrated that **39** was selectively hydrolyzed by MMP-2 and MMP-expressing cells. **40** was evaluated *in vitro* with HT1080 cells or MCF-7 cells cultured 48h in serum-free medium. HT1080 cells exhibited strong fluorescence contrary to MCF-7 cells. Addition of MMP-2 to MCF-7 cells led to a retention of fluorescence at the MCF-7 cells. Treatment of HT1080 cells with 10  $\mu$ M 1,10-phenanthroline resulted in a substantial 10-fold lower fluorescent signal. Both TIMP-1 (soluble endogenous MMP inhibitor) and TIMP-2 (membrane-anchored and soluble MMP inhibitor) reduced the TMR fluorescence in HT1080 cells. **40** was tested in mice bearing HT1080 and MCF-7 tumors. Retention of **40** was observed in HT1080 tumors, with the highest uptake 60 min p.i., but not in MCF-7 tumors. Moreover, the fluorescent signal of HT1080 tumor slices was correlated with the fluorescent staining of MMP-2. **41** was tested *in vitro* and accumulated significantly higher in HT1080 cells than in MCF-7 cells. Furthermore, addition of 10  $\mu$ M 1,10-phenanthroline decreased substantially the retention of **41** in HT1080 cells. *In vivo* evaluation in mice bearing HT1080 and MCF-7 tumors showed a retention of **41** in HT1080 tumors, with the highest intensity 60 min p.i., contrary to MCF-7 tumors. Treatment with 20 mg/kg/day of 1,10-phenanthroline three days before the microPET scan resulted in 1.3-, 3.6- and 3.3-fold higher uptake of HT1080 tumors than MCF-7 tumors at 15, 60 and 120 min. *Ex vivo* biodistribution data were in accordance with *in vivo* experiments. Thus, **41** allowed visualizing specifically MMP-expressing tumors *in vivo*.

**[<sup>64</sup>Cu]-BBQ650-PLGVR-K(Cy5.5)-E-K(DOTA)-OH, 42**

Huang *et al.* [75] developed an activatable dual modality (PET/fluorescent) imaging agent **42** (Fig. 21) which consists of three parts: first of all, a MMP cleavable peptide sequence PLGVR, which is specially cleaved by MMP-7, -9, -12 and -13. Besides, **42** includes a pair of dye/quencher, with NIR Cy5.5 as a dye and

42

BBQ650 as a fluorescence quencher group, which is nonfluorescent. Finally, the peptide was conjugated with DOTA for radiolabelling with <sup>64</sup>Cu. **42** exhibited quite high stability in PBS and mouse serum at 37°C for up to 24 hr. BBQ650-PLGVR-K(Cy5.5)-E-K(DOTA)-OH was evaluated for its cleavage specificity by MMP-13 enzyme *in vitro*. The fluorescent intensity of this probe was time dependent, the signal has an 8.2-fold increase from 0 to 120 min, which was blocked in the presence of a broad-spectrum MMP inhibitor (MMP inhibitor III). This fluorescent probe was tested in mice bearing U87MG human glioma xenograft tumors. The U87MG tumor was clearly visualized with high tumor-to-background contrast. Besides, the fluorescence intensity increased during the scanning period. Preinjection with the MMP inhibitor III led to a lower intensity at the tumor site at each time point, which suggests specific uptake of this fluorescent probe. Due to the limited spatial resolution of NIRF, the quantitative technique PET was used in order to correct the enzyme activity obtained from optical imaging. In one mouse was injected the same amount of MMP-13 enzyme at four different sites. At sites 1 and 3 were injected 15  $\mu$ Ci of **42** whereas at sites 2 and 4 were administered 2.5  $\mu$ Ci of **42**. Coinjection of the MMP inhibitor III was performed at site 3 and 4. By considering the optical signal, the blocking effects were 38.33% for site 1 vs site 3 and 10.66% for site 2 vs site 4. By normalization of the fluorescence signal per unit of radioactivity, the real fluorescent signal at each inhibition site was calculated. The inhibition percentages at site 3 and site 4 were 79.6% and 79.7%, respectively. The blocking effect was more accurately quantified after the coregistration of PET/fluorescence signals. To conclude, **42** allowed specific visualization of U87MG tumors *in vivo*. Moreover, the quantitative PET signal allowed correction of the enzyme activity determined from optical imaging.

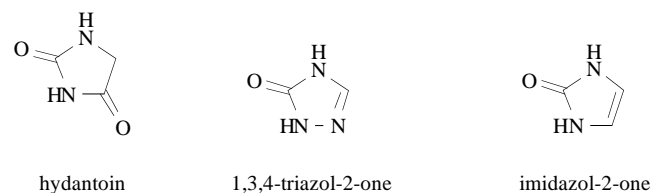


Fig. (22). Structure of alternative ZBGs to the hydroxamate.

**Table 4. clog P, log P, clog D and log D Values of Synthetic MMP Inhibitors/MMP Peptides**

MMP inhibitors / MMP peptides	clog P	log P	clog D	log D
<b>RP805</b>	2.53			
<b>6a</b> [40]; [41]	0.228			
<b>7</b> [42]; [43]	4.24			
<b>8</b> [44]; [45]	3.76			
<b>9</b> [46]	3.09			
<b>10</b> [48]	3.89			
<b>12a</b> [50]; [51]				2.02
<b>13a</b> [48]	2.40			
<b>13b</b> [48]	2.40			
<b>13c</b> [48]	1.79			
<b>13d</b> [48]	1.97			
<b>13e</b> [48]	1.97			
<b>14a</b> [53]	2.37			
<b>14b</b> [53]	2.37			
<b>14c</b> [53]	2.64			
<b>14d</b> [53]	2.94			
<b>14e</b> [53]	2.94			
<b>14f</b> [53]	2.59			
<b>14g</b> [53]	3.09			
<b>14h</b> [53]	3.09			
<b>14i</b> [53]	3.35			
<b>15a</b> [54]	1.40			
<b>15d</b> [54]	0.14			
<b>16</b> [51]; [56]				1.34
<b>17</b> [50]; [57]				1.85
<b>18</b> [53]				0.60
<b>19</b> [47]	3.80			
<b>20a</b> [59]	3.46			
<b>20b</b> [59]	4.02			
<b>20c</b> [59]	4.02			
<b>20d</b> [59]	4.23			
<b>20e</b> [59]	4.23			
<b>20f</b> [59]	4.23			
<b>20g</b> [59]	3.90			
<b>22</b> [60]	2.88			
<b>23</b> [42]; [43]	5.48			

(Table 4) Contd....

MMP inhibitors / MMP peptides	clog P	log P	clog D	log D
24 [44]; [45]	5.00			
25a [61]	3.58			
25b [61]	3.80			
25c [62]	2.80			
25d [62]	4.06			
26 [63]	3.80			
27 [65]	4.21			
28 [66]			2.88	2.15
29 [67]			0.99	0.78
31 [69]		0.36		
34 [71]		4.0		
35 [72]				-3.6

## PERSPECTIVES AND CONCLUSION

### In Vivo Models for the Evaluation of the MMP-targeting Probes

The regional distribution of radiolabelled MMPs has been rather well-characterized in vascular imaging, particularly atherosclerotic lesions and aneurysm. [<sup>111</sup>In]-DTPA-RP782 **3**, [<sup>99m</sup>Tc]- (HYNIC-RP805)(tricine)(TPPTS) **5**, and [<sup>123</sup>I]I-HO-CGS 27023A **15e** exhibited specific binding in the aforementioned diseases. So far, most preclinical evaluation of radiolabelled MMPs occurred only at the preliminary stage. The signal to noise ratios of most probes were rather low and comparisons of probe binding with *ex vivo* characterization of target expression (IHC or zymography) were rarely performed. Some work has been done in tumor models but very little work was done in models of inflammation (asthma, COPD, rheumatoid arthritis, etc). There is much opportunity for tracer evaluation in disease models other than atherosclerosis or aneurysm.

### Specific Activity

A high specific radioactivity of PET/SPECT probes may be required considering that natural TIMPs bind to the same domain as MMPs [76] with a very high affinity in the picomolar range. TIMP competition for probe binding is probably severe since most radiolabelled MMPs have affinities in the nanomolar range with exception of the recently published compound **18**. If possible, biological samples or experimental animals should be depleted of TIMPs because TIMPs tightly and irreversibly bind to active MMPs and will decrease the uptake of the radiolabelled probes. However, if radiolabelled MMPs would visualize the net balance of MMPs not occupied by TIMPs, this fraction might be a clinically important parameter, which could reflect the protease activity in the extracellular matrix.

### Affinity

The IC<sub>50</sub> values of the reported synthetic MMP inhibitors and MMP peptides are summarized in (Table 3). The parent compound of [<sup>99m</sup>Tc]- (HYNIC-RP805)(tricine)(TPPTS) **5**, RP805, exhibited affinity in the low nanomolar range. Since [<sup>99m</sup>Tc]-labelled RP805 displayed specific binding *in vivo* and since the labeled probe probably has a decreased affinity compared to the parent com-

pound, a nanomolar probe affinity appears sufficient for SPECT imaging, at least in cardiovascular diseases.

### Lipophilicity

The clog P, log P, clog D and log D of the reported synthetic MMP inhibitors and MMP peptides are reviewed in (Table 4). As two third of MMPs are soluble, it is more logical to develop a hydrophilic MMP. Moreover, some radiolabelled probes with a very high log P values such as **23** (5.48) which were developed have shown a very strong non-specific binding. Thus, log P values greater than 2.5 may better be avoided.

### Alternative to Hydroxamic Acid

Agrawal *et al.* [77] demonstrated the importance of the ZBG for MMPs and as a result, modification of the ZBG has more effect than change of the substituents in the different pockets. So much effort has to be focused on the development of alternative ZBGs. Even though the hydroxamic acid is a potent ZBG, it has some drawbacks such as a difficult synthesis, metabolic instability and most importantly, a too high potency for zinc binding. Indeed the hydroxamate binds many zinc proteases and can also chelate metals other than zinc such as iron (hydroxamates bind Fe(III) 10<sup>6</sup> to 10<sup>11</sup>-fold stronger than Zn(II)). Other ZBGs which are more selective than hydroxamic acid have been designed and developed such as hydantoins, 1,3,4-triazol-2-ones and imidazol-2-ones (Fig. 22); [78] but labelled probes based on these structures were not yet tested *in vivo*.

### Pro/active MMP Binding

Many MMPs bind to both active and pro-MMPs, for instance **7**, thus the binding of most MMP is not activity-dependent. Therefore the use of radiolabeled substrates [79], antibodies (e.g. [<sup>99m</sup>Tc]-anti-MT1-MMP mAb [80]; [81]; [82]) or cell-penetrating peptides [83] should be considered as alternatives for MMP imaging. A complementary approach with a MMP and a MMP antibody could also be performed to target the activity and the density of MMPs.

To conclude, there is much opportunity to design, synthesize and evaluate a new generation of probes targeting MMPs.



**CONFLICT OF INTEREST**

The authors confirm that this article content has no conflicts of interest.

**ACKNOWLEDGEMENTS**

The authors wish to thank the Dutch Technology Foundation (STW) for financial support (project 08008)

**ABBREVIATIONS**

AA5	=	Annexin A5
ADAM	=	A disintegrin and metalloproteinase
ApoE-/-	=	Apolipoprotein E
COPD	=	Chronic obstructive pulmonary disease
DOTA	=	1,4,7,10-tetraazacyclododecane-1,4,7,10-Tetraacetic acid
DTPA	=	Diethylene triamine pentaacetic acid (or Pentetic acid)
ECM	=	Extracellular matrix
EGF	=	Epidermal Growth Factor
FITC	=	fluorescein isothiocyanate
HC	=	High-cholesterol
HYNIC	=	hydrazinonicotinamide
ID/g	=	Injected dose/gram
IVC	=	Inferior vena cava
LDLr-/-	=	Low-density-lipoprotein receptor
LV	=	Left ventricular
MADDAM	=	Metalloprotease and disintegrin dendritic antigen marker
MI	=	Myocardial infarction
MMP	=	Matrix metalloproteinase
MMPI	=	Matrix metalloproteinase inhibitor
MRI	=	Magnetic resonance imaging
ND	=	Not determined
NIR	=	Near infrared
PBS	=	Phosphate-buffered saline
PET	=	Positron emission tomography
qRT-PCR	=	Quantitative real time polymerase chain reaction
RCY	=	Radiochemical yield
SAR	=	Structure-activity relationships
SPECT	=	Single photon emission computed tomography
SUV	=	Standardized uptake value
TACE	=	TNF alpha protease inhibitor
TIMP	=	Tissue inhibitor of matrix metalloproteinase
(t)MDC	=	(Transmembrane) metalloprotease-like, disintegrin-like, cystein-rich protein
TMR	=	Tetramethylrhodamine
TNF	=	Tumor necrosis factor
TPPTS	=	Trisodium triphenylphosphine-3,3',3''-trisulfonate
TUNEL	=	Terminal deoxyribonucleotide transferase-mediated nick-end labeling
WT	=	Wild-type
ZBG	=	Zinc binding group

**REFERENCES**

- Seals DF, Courtneidge SA. The ADAMs family of metalloproteases: multidomain proteins with multiple functions. *Genes & Development* 2003; 17(1): 7-30.
- Hooper NM. Families of zinc metalloproteases. *FEBS Letters* 1994; 354: 0-5.
- Stöcker W, Bode W. Structural features of a superfamily of zinc-endopeptidases: the metzincins. *Curr Opin in Structural Biol* 1995; 5: 383-90.
- Nagase H, Woessner JF. Matrix metalloproteinases. *J Biological Chemistry* 1999; 274(31): 21491-4.
- Overall CM. Molecular Determinants of Metalloproteinase Substrate Specificity 2002; 22(604): 657-672.
- White JM. ADAMs: modulators of cell-cell and cell-matrix interactions. *Curr Opin Cell Biol* 2003; 15(5): 598-606.
- MacFadyen RJ. Can matrix metalloproteinase inhibitors provide a realistic therapy in cardiovascular medicine? *Curr Opin Pharmacol* 2007; 7(2): 171-8.
- Browner MF, Smith WW, Castelhana a L. Matrilysin-inhibitor complexes: common themes among metalloproteases. *Biochemistry* 1995; 34(20): 6602-10.
- Scherer RL, McIntyre JO, Matrisian LM. Imaging matrix metalloproteinases in cancer. *Cancer Metastasis Rev* 2008; 27(4): 679-90.
- Hu J, Van den Steen PE, Sang Q-X A, Opdenakker G. Matrix metalloproteinase inhibitors as therapy for inflammatory and vascular diseases. *Nat Rev Drug Discovery* 2007; 6(6): 480-98.
- Whittaker M, Floyd CD, Brown P, Gearing AJH. Design and therapeutic application of matrix metalloproteinase inhibitors. *Chemical Rev* 1999; 99(9): 2735-76.
- Hidalgo M, Eckhardt SG. Development of matrix metalloproteinase inhibitors in cancer therapy. *J Natl Cancer Institute* 2001; 93(3): 178-93.
- Konstantinopoulos PA, Karamouzis MV, Papatsoris AG, Papavasiliou AG. Matrix metalloproteinase inhibitors as anticancer agents. *Int J Biochem Cell Biol* 2008; 40(6-7): 1156-68.
- Bremer C, Bredow S, Mahmood U. *et al.* Optical Imaging of Matrix Metalloproteinase - 2 Activity in Tumors: Feasibility Study in a Mouse Model. *Radiology* 2001; 221(2): 523-9.
- Hutton M, Willenbrock F, Brocklehurst K, Murphy G. Kinetic analysis of the mechanism of interaction of full-length TIMP-2 and gelatinase A: evidence for the existence of a low-affinity intermediate. *Biochemistry* 1998; 37(28): 10094-8.
- Murphy G, Willenbrock F. Tissue inhibitors of matrix metalloendopeptidases. *Methods Enzymol* 1995; 248: 496-511.
- Verma RP, Hansch C. Matrix metalloproteinases (MMPs): chemical-biological functions and (Q)SARs. *Bioorganic Med Chem* 2007; 15(6): 2223-68.
- Sheppeck JE, Gilmore JL, Tebben A, *et al.* Hydantoins, triazolones, and imidazolones as selective non-hydroxamate inhibitors of tumor necrosis factor-alpha converting enzyme (TACE). *Bioorganic Med Chem Letters* 2007; 17(10): 2769-74.
- Stocker W, Bode W. Structural features of a superfamily of zinc-endopeptidases: the metzincins. *Curr Opin Structural Biol* 1995; 5: 383-390.
- Tung CH, Mahmood U, Bredow S, Weissleder R. *In vivo* imaging of proteolytic enzyme activity using a novel molecular reporter. *Cancer Res* 2000; 60(17): 4953-8.
- Williamson R a, Marston F a, Angal S, *et al.* Disulphide bond assignment in human tissue inhibitor of metalloproteinases (TIMP). *Biochem J* 1990; 268(2): 267-74.
- Murphy G, Houbrechts a, Cockett MI, Williamson RA, O'Shea M, Docherty AJ. The N-terminal domain of tissue inhibitor of metalloproteinases retains metalloproteinase inhibitory activity. *Biochemistry* 1991; 30(33): 8097-102.
- Yang SW, Chanda D, Cody JJ, *et al.* Conditionally replicating adenovirus expressing TIMP2 increases survival in a mouse model of disseminated ovarian cancer. *PLoS One* 2011; 6(10): e25131.
- Giersing BK, Rae MT, CarballidoBrea M, Williamson R a, Blower PJ. Synthesis and characterization of 111In-DTPA-N-TIMP-2: a radiopharmaceutical for imaging matrix metalloproteinase expression. *Bioconjugate Chemistry* 2001; 12(6): 964-71.
- Kulasegaram R, Giersing B, Page CJ, *et al.* *In vivo* evaluation of 111 In-DTPA- N -TIMP-2 in Kaposi sarcoma associated with HIV infection. *European J Nuclear Med Mol Imaging* 2001; 28(6): 756-761.

- [26] Oltenfreiter R, Burvenich I, Staelens L, *et al.* Synthesis, quality control and *in vivo* evaluation of [<sup>123</sup>I] rhTIMP-2, a potential tumour-imaging agent. *J Labelled Compounds Radiopharm* 2005; 48(5): 387-396.
- [27] Van Steenkiste M, Oltenfreiter R, Frankenne F, *et al.* Membrane type 1 matrix metalloproteinase detection in tumors, using the iodinated endogenous [<sup>123</sup>I]-tissue inhibitor 2 of metalloproteinases as imaging agent. *Cancer Biotherapy Radiopharm* 2010; 25(5): 511-20.
- [28] Codd R. Traversing the coordination chemistry and chemical biology of hydroxamic acids. *Coordination Chemistry Rev* 2008; 252(12-14): 1387-1408.
- [29] Su H, Spinale FG, Dobrucki LW, *et al.* Noninvasive targeted imaging of matrix metalloproteinase activation in a murine model of postinfarction remodeling. *Circulation* 2005; 112(20): 3157-67.
- [30] Zhang J, Nie L, Razavian M, *et al.* Molecular imaging of activated matrix metalloproteinases in vascular remodeling. *Circulation* 2008; 118(19): 1953-60.
- [31] Tavakoli S, Razavian M, Zhang J, *et al.* Matrix metalloproteinase activation predicts amelioration of remodeling after dietary modification in injured arteries. *Arteriosclerosis, Thrombosis, Vascular Biol* 2011; 31(1): 102-9.
- [32] Sahul ZH, Mukherjee R, Song J, *et al.* Targeted imaging of the spatial and temporal variation of matrix metalloproteinase activity in a porcine model of postinfarct remodeling: relationship to myocardial dysfunction. *Circulation. Cardiovascular Imaging* 2011; 4(4): 381-91.
- [33] Fujimoto S, Hartung D, Ohshima S, *et al.* Molecular imaging of matrix metalloproteinase in atherosclerotic lesions: resolution with dietary modification and statin therapy. *J Am College Cardiol* 2008; 52(23): 1847-57.
- [34] Ohshima S, Petrov A, Fujimoto S, *et al.* Molecular imaging of matrix metalloproteinase expression in atherosclerotic plaques of mice deficient in apolipoprotein or low-density-lipoprotein receptor. *J Nuclear Med* 2009; 50(4): 612-7.
- [35] Ohshima S, Fujimoto S, Petrov A, *et al.* Effect of an antimicrobial agent on atherosclerotic plaques: assessment of metalloproteinase activity by molecular imaging. *J Am College Cardiol* 2010; 55(12): 1240-9.
- [36] Razavian M, Tavakoli S, Zhang J, *et al.* Atherosclerosis Plaque Heterogeneity and Response to Therapy Detected by *In vivo* Molecular Imaging of Matrix Metalloproteinase Activation. *J Nuclear Medicine* 2011; 52: 1795-1802.
- [37] Haider N, Hartung D, Fujimoto S, *et al.* Dual molecular imaging for targeting metalloproteinase activity and apoptosis in atherosclerosis: molecular imaging facilitates understanding of pathogenesis. *J Nuclear Cardiol* 2009; 16(5): 753-62.
- [38] Tekabe Y, Li Q, Luma J, *et al.* Noninvasive monitoring the biology of atherosclerotic plaque development with radiolabeled annexin V and matrix metalloproteinase inhibitor in spontaneous atherosclerotic mice. *J Nuclear Cardiol* 2010; 17(6): 1073-81.
- [39] Razavian M, Zhang J, Nie L, *et al.* Molecular imaging of matrix metalloproteinase activation to predict murine aneurysm expansion *in vivo*. *J Nuclear Med* 2010; 51(7): 1107-15.
- [40] Bellac CL, Li Y, Lou Y, *et al.* Novel MMP inhibitor [18F]-Marimastat-aryltrifluoroborate as a probe for *in vivo* PET imaging in cancer. *Cancer Res* 2010; 70(19): 7562-9.
- [41] Li Y, Ting R, Harwig CW, *et al.* Towards kit-like 18F-labeling of marimastat, a noncovalent inhibitor drug for *in vivo* PET imaging cancer associated matrix metalloproteinases. *MedChemComm* 2011; 2(10): 925-1022.
- [42] Oltenfreiter R, Staelens L, Lejeune A, *et al.* New radioiodinated carboxylic and hydroxamic matrix metalloproteinase inhibitor tracers as potential tumor imaging agents. *Nuclear Med Biology* 2004; 31(4): 459-68.
- [43] Oltenfreiter R, Staelens L, Labied S, *et al.* Tryptophane-Based Biphenylsulfonamide Matrix Metalloproteinase Inhibitors as Tumor Imaging Agents. *Cancer Biotherapy Radiopharm* 2005; 20(6): 639-48.
- [44] Oltenfreiter R, Staelens L, Kersemans V, *et al.* Valine-based biphenylsulfonamide matrix metalloproteinase inhibitors as tumor imaging agents. *Applied Radiation Isotopes* 2006; 64(6): 677-85.
- [45] Oltenfreiter R, Staelens L, Hillaert U, *et al.* Synthesis, radiosynthesis, *in vitro* and preliminary *in vivo* evaluation of biphenyl carboxylic and hydroxamic matrix metalloproteinase (MMP) inhibitors as potential tumor imaging agents. *Applied Radiation Isotopes* 2005; 62(6): 903-13.
- [46] Fei X, Zheng Q-H, Liu X, *et al.* Synthesis of MMP inhibitor radiotracer [<sup>11</sup>C]CGS 25966, a new potential pet tumor imaging agent. *J Labelled Compounds and Radiopharm* 2003; 46(4): 343-51.
- [47] Zheng Q-H, Fei X, Liu X, *et al.* Comparative studies of potential cancer biomarkers carbon-11 labeled MMP inhibitors (S)-2-(4'-[<sup>11</sup>C]methoxybiphenyl-4-sulfonylamino)-3-methylbutyric acid and N-hydroxy-(R)-2-[[4'-[<sup>11</sup>C]methoxyphenyl)sulfonyl]benzylamino]-3-methylbutanamide. *Nuclear Med Biol* 2004; 31(1): 77-85.
- [48] Fei X, Zheng Q-H, Hutchins GD, *et al.* Synthesis of MMP inhibitor radiotracers [<sup>11</sup>C]methyl-CGS 27023A and its analogs, new potential PET breast cancer imaging agents. *J Labelled Compounds Radiopharm* 2002; 45(6): 449-70.
- [49] MacPherson LJ, Bayburt EK, Capparelli MP, *et al.* Discovery of CGS 27023A, a non-peptidic, potent, and orally active stromelysin inhibitor that blocks cartilage degradation in rabbits. *J Med Chem* 1997; 40(16): 2525-32.
- [50] Wagner S, Law MP, Faust A, Ho C, Schro S. Novel Fluorinated Derivatives of the Broad-Spectrum MMP Inhibitors N-Hydroxy-2(R)-[[4-methoxyphenyl)sulfonyl](benzyl)- and (3-picolyl)-amino]-3-methyl-butanamide as Potential Tools for the Molecular Imaging of Activated MMPs with PET. *J Med Chem* 2007; 2: 5752-64.
- [51] Breyholz HJ, Wagner S, Levkau B, Schober O, Kopka K. A [<sup>18</sup>F]-radiolabeled analogue of CGS 27023A as a potential agent for assessment of matrix-metalloproteinase activity *in vivo*. *J Nucl Med Mol Imaging* 2007; 51: 24-32.
- [52] Wagner S, Faust A, Breyholz H-J, Schober O, Schäfers M, Kopka K. The MMP inhibitor (R)-2-(N-benzyl-4-(2-[<sup>18</sup>F]fluoroethoxy)phenylsulphonamido)-N-hydroxy-3-methylbutanamide: Improved precursor synthesis and fully automated radiosynthesis. *Applied Radiation Isotopes* 2011; 69(6): 862-8.
- [53] Zheng Q-H, Fei X, Liu X, *et al.* Synthesis and preliminary biological evaluation of MMP inhibitor radiotracers [<sup>11</sup>C]methyl-halo-CGS 27023A analogs, new potential PET breast cancer imaging agents. *Nuclear Med Biol* 2002; 29(7): 761-70.
- [54] Kopka K, Wagner S, Law MP, *et al.* Synthesis and preliminary biological evaluation of new radioiodinated MMP inhibitors for imaging MMP activity *in vivo*. *Nuclear Med Biol* 2004; 31: 257-267.
- [55] Schäfers M, Riemann B, Kopka K, *et al.* Scintigraphic imaging of matrix metalloproteinase activity in the arterial wall *in vivo*. *Circulation* 2004; 109(21): 2554-9.
- [56] Kopka K, Schober O, Wagner S. (18F)-labelled cardiac PET tracers: selected probes for the molecular imaging of transporters, receptors and proteases. *Basic Res Cardiology* 2008; 103(2): 131-43.
- [57] Wagner S, Breyholz H-J, Hölte C, *et al.* A new 18F-labelled derivative of the MMP inhibitor CGS 27023A for PET: radiosynthesis and initial small-animal PET studies. *Applied Radiation Isotopes* 2009; 67(4): 606-10.
- [58] Hugenberg V, Breyholz H-jörg, Riemann B, *et al.* A new class of highly potent matrix metalloproteinase inhibitors based on triazole-substituted hydroxamates: (Radio)synthesis, *in vitro* and first *in vivo* evaluation. *J Med Chem* 2012; 55(10): 4714-27.
- [59] Fei X, Zheng Q-H, Liu X, *et al.* Synthesis of radiolabeled biphenylsulfonamide matrix metalloproteinase inhibitors as new potential PET cancer imaging agents. *Bioorganic Med Chem Letters* 2003 Jul; 13(13): 2217-22.
- [60] Kuhnast B, Bodenstein C, Wester HJ, Weber W. Carbon-11 labeling of anN-sulfonylamino acid derivative: a potential tracer for MMP-2 and MMP-9 imaging. *J Labelled Compounds Radiopharm* 2003; 46(6): 539-53.
- [61] Furumoto S, Takashima K, Kubota K, Ido T, Iwata R, Fukuda H. Tumor detection using 18F-labeled matrix metalloproteinase-2 inhibitor. *Nuclear Med Biol* 2003; 30(2): 119-25.
- [62] Furumoto S, Iwata R, Ido T. Design and synthesis of fluorine-18 labeled matrix metalloproteinase inhibitors for cancer imaging. *J Labelled Compounds Radiopharm* 2002; 45(11): 975-86.
- [63] Zheng Q-H, Fei X, DeGrado TR, *et al.* Synthesis, biodistribution and micro-PET imaging of a potential cancer biomarker carbon-11 labeled MMP inhibitor (2R)-2-[[4-(6-fluorohex-1-

- nyl)phenyl]sulfonylamino]-3-methylbutyric acid [<sup>11</sup>C]methyl ester. *Nuclear Med Biol* 2003; 30(7): 753-60.
- [65] Sheppeck JE, Gilmore JL, Tebben A, *et al.* Hydantoins, triazolones, and imidazolones as selective non-hydroxamate inhibitors of tumor necrosis factor-alpha converting enzyme (TACE). *Bioorganic Med Chem Letters* 2007; 17(10): 2769-74.
- [66] Breyholz H-J, Schäfers M, Wagner S, *et al.* C-5-disubstituted barbiturates as potential molecular probes for noninvasive matrix metalloproteinase imaging. *J Med Chem* 2005; 48(9): 3400-9.
- [67] Breyholz H-J, Wagner S, Faust A, *et al.* Radiofluorinated pyrimidine-2,4,6-triones as molecular probes for noninvasive MMP-targeted imaging. *ChemMedChem* 2010; 5(5): 777-89.
- [68] Schritgen D, Breyholz H-J, Wagner S, *et al.* A New Generation of Radiofluorinated Pyrimidine-2,4,6-triones as MMP-Targeted Radiotracers for Positron Emission Tomography. *J Med Chem* 2012; 55(1): 223-32.
- [69] Claesener M, Schober O, Wagner S, Kopka K. Radiosynthesis of a <sup>68</sup>Ga labeled matrix metalloproteinase inhibitor as a potential probe for PET imaging. *Applied Radiation Isotopes* 2012; 70(8): 1723-28.
- [70] Koivunen E, Arap W, Valtanen H, *et al.* Tumor targeting with a selective gelatinase inhibitor. *Nature Biotechnology* 1999; 17(8): 768-74.
- [71] Kuhnast B, Bodenstern C, Haubner R, *et al.* Targeting of gelatinase activity with a radiolabeled cyclic HWGF peptide. *Nuclear Med Biol* 2004; 31(3): 337-44.
- [72] Sprague JE, Li WP, Liang K, Achilefu S, Anderson CJ. *In vitro* and *in vivo* investigation of matrix metalloproteinase expression in metastatic tumor models. *Nuclear Med Biol* 2006; 33(2): 227-37.
- [73] Hanaoka H, Mukai T, Habashita S, *et al.* Chemical design of a radiolabeled gelatinase inhibitor peptide for the imaging of gelatinase activity in tumors. *Nuclear Med Biol* 2007; 34(5): 503-10.
- [74] Ujula T, Huttunen M, Luoto P, *et al.* Matrix metalloproteinase 9 targeting peptides: syntheses, <sup>68</sup>Ga-labeling, and preliminary evaluation in a rat melanoma xenograft model. *Bioconjugate Chem* 2010; 21(9): 1612-21.
- [75] Cheng TL, Chuang CH, Chuang KH, *et al.* *In vivo* positron emission tomography imaging of protease activity by generation of a hydrophobic product from a non-inhibitory protease substrate. *Clinical Cancer Res* 2012; 18(1): 238-47.
- [76] Huang CW, Li Z, Conti PS. Radioactive smart probe for potential corrected matrix metalloproteinase imaging. *Bioconjugate Chem* 2012; 23(11): 2159-67.
- [77] Murphy, G. Tissue inhibitors of metalloproteinases. *Genome Biol* 2011; 12(233): 1-7.
- [78] Agrawal A, Romero-Perez D, Jacobsen JA, Villarreal FJ, Cohen SM. Zinc-binding groups modulate selective inhibition of MMPs. *ChemMedChem* 2008; 3(5): 812-20.
- [79] Sheppeck JE, Gilmore JL, Tebben A, *et al.* Hydantoins, triazolones, and imidazolones as selective non-hydroxamate inhibitors of tumor necrosis factor-alpha converting enzyme (TACE). *Bioorganic Med Chem Letters* 2007; 17(10): 2769-74.
- [80] Pfaffen S, Frey K, Stutz I, Roesli C, Neri D. Tumour-targeting properties of antibodies specific to MMP-1A, MMP-2 and MMP-3. *Eur J Nuclear Med and Molecular Imaging* 2010; 37(8): 1559-65.
- [81] Temma T, Sano K, Kuge Y, *et al.* Development of a radiolabeled probe for detecting membrane type-1 matrix metalloproteinase on malignant tumors. *Biological Pharmaceutical Bulletin* 2009; 32(7): 1272-7.
- [82] Kuge Y, Takai N, Ogawa Y, *et al.* Imaging with radiolabelled anti-membrane type 1 matrix metalloproteinase (MT1-MMP) antibody: potentials for characterizing atherosclerotic plaques. *Eur J Nuclear Med Mol Imaging* 2010; 37(11): 2093-104.
- [83] Watkins G, Jones EF, Scott Shell M, *et al.* Development of an optimized activatable MMP-14 targeted SPECT imaging probe. *Bioorganic Med Chem* 2009; 17(2): 653-9.
- [84] van Duijnhoven SMJ, Robillard MS, Nicolay K, Grüll H. Tumor targeting of MMP-2/9 activatable cell-penetrating imaging probes is caused by tumor-independent activation. *J Nuclear Med* 2011; 52(2): 279-86.